Modulation of fungal phosphate homeostasis by the plant hormone strigolactone

James M Bradley, Michael Bunsick, George Ly, Bruno Aquino, Flora Zhiqi Wang, Duncan Holbrook-Smith, Shingo Suginoo, Dylan Bradizza, Naoki Kato, Omar As'sadiq, et al.

Modulation of fungal phosphate homeostasis by the plant hormone strigolactone

Authors:
James M. Bradley[1,†], Michael Bunsick[1,†], George Ly[1,†], Bruno Aquino[1,†], Flora Zhiqi Wang[1], Duncan Holbrook-Smith[2], Shingo Suginoo[3], Dylan Bradizza[1], Naoki Kato[4], Omar As'sadiq[1], Nina Marsh[1], Hiroyuki Osada[4], François-Didier Boyer[5], Christopher S. P. McErlean[6], Yuichiro Tsuchiya[7], Rajagopal Subramaniam[8], Dario Bonetta[9], Peter McCourt[1,10,*] and Shelley Lumba[1,10,*]

Affiliations:
[1] Department of Cell & Systems Biology, University of Toronto, 25 Willcocks Street, Toronto, ON, M5S 3B2, Canada.
[2] Institute of Molecular Systems Biology, ETH, Zurich, Switzerland.
[3] Department of Biological Science, Graduate School of Science, Nagoya University, Furo-cho, Chikusa, Nagoya, Japan, 464-8601.
[4] RIKEN Center for Sustainable Research Science, 2-1 Hirosawa, Wako, Saitama 351-0198, Japan
[5] Université Paris-Saclay, CNRS, Institut de Chimie des Substances Naturelles, UPR 2301, 91198, Gif-sur-Yvette, France.
[6] School of Chemistry, The University of Sydney, NSW 2006, Australia.
[7] Institute of Transformative Bio-Molecules, Nagoya University, Furo-cho, Chikusa-ku, Nagoya 464-8602, Japan.
[8] Agriculture and Agri-Food Canada, Ottawa, Ontario, Canada
[9] Ontario Tech University, 2000 Simcoe St N, Oshawa, ON, L1G 0C5, Canada.
[10] Centre for the Analysis of Genome Evolution and Function, University of Toronto, 25 Willcocks Street, Toronto, ON, M5S 3B2, Canada.

[†] These authors contributed equally to this work.
* To whom correspondences should be addressed

*e-mail: Shelley Lumba <shelley.lumba@utoronto.ca> **Lead contact**
*e-mail: Peter McCourt <peter.mccourt@utoronto.ca>
e-mail: James Bradley <james.bradley@utoronto.ca>
e-mail: Michael Bunsick <michael.bunsick@mail.utoronto.ca>
e-mail: George Ly <george.ly@mail.utoronto.ca>
e-mail: Bruno Aquino <bruno.aquino@utoronto.ca>
e-mail: Flora Zhiqi Wang <florazhiqiwang@berkeley.edu>
e-mail: Duncan Holbrook-Smith <dholbrooksmith89@gmail.com>
e-mail: Shingo Suginoo < sugino.shingo.u8@s.mail.nagoya-u.ac.jp>
e-mail: Dylan Bradizza <dylan.bradizza@mail.utoronto.ca>
e-mail: Naoki Kato <naoki.kato@setsunan.ac.jp>
e-mail: Omar As'sadiq <omar.assadiq@mail.utoronto.ca>
e-mail: Nina Marsh <nina.marsh@mail.utoronto.ca>
e-mail: Hiroyuki Osada <osadahiro@riken.jp>
e-mail: François-Didier Boyer <Francois-Didier.BOYER@cnrs.fr>
e-mail: Christopher McErlean <christopher.mcerlean@sydney.edu.au>
e-mail: Tsuchiya Yuichiro <yuichiro@itbm.nagoya-u.ac.jp>
e-mail: Subramaniam Rajagopal <rajagopal.subramaniam@agr.gc.ca>

e-mail: Dario Bonetta <dario.bonetta@uoit.ca>

SUMMARY

Inter-kingdom communication through small molecules is essential to the coexistence of organisms in an ecosystem. In soil communities, the plant root is a nexus of interactions for a remarkable number of fungi and is a source of small molecule plant hormones that shape fungal compositions. Although hormone signaling pathways are established in plants, how fungi perceive and respond to molecules is unclear because many plant-associated fungi are recalcitrant to experimentation. Here, we develop an approach using the model fungus, *Saccharomyces cerevisiae*, to elucidate mechanisms of fungal response to plant hormones. Two plant hormones, strigolactone and methyl jasmonate produce unique transcript profiles in yeast affecting phosphate and sugar metabolism, respectively. Genetic analysis in combination with structural studies suggest SLs require the high affinity transporter, Pho84, to modulate phosphate homeostasis. The ability to study small molecule plant hormones in a tractable genetic system should have utility in understanding fungal-plant interactions.

Keywords: Chemical communication, Interspecies sensing, *Saccharomyces cerevisiae*, Strigolactone, Jasmonate, Genetic analysis, Plant hormone signaling, Fungal kingdom, Chemical ecology

INTRODUCTION

Organisms seldom live in isolation and are exposed to a myriad of molecules released by other organisms during their lifecycle. Consequently, the success of any organism within an ecosystem partly relies on their capacity to perceive and respond to these inter-organismal signals, which are often encoded by small molecules. In prokaryotes, for example, secreted small molecules dictate population densities both within and between species.[1] In eukaryotes, many insect-insect and insect-plant interactions use small molecules as chemical attractants or repellents for social interactions.[2,3] An astonishing number of inter-kingdom associations also occurs between plants and their microbiome (bacteria) as well as plants and their mycobiome (fungi); however, only a few small molecules have been linked to these associations.[4,5,6] Curiously, plant hormones (phytohormones), which normally regulate plant growth and development, appear to be an important class of small molecules that influence both the micro- and mycobiome associations with plants, particularly in the soil around the root (rhizosphere).

Eight phytohormones have been characterized and of these, strigolactones (SLs), jasmonic acid (JA), auxins, gibberellins (GA), abscisic acid (ABA), cytokinins (CKs), and salicylic acid (SA) are detected in the soil at varying concentrations (**Figure 1A**).[7,8] Although plants are the major contributor of phytohormone levels in the rhizosphere, many soil bacteria[9,10,11] and fungi[12,13] also make these small molecules. Composition and levels of phytohormone in the soil are therefore transient and dynamic depending on species composition, developmental stage, and presence of particular genotypes from all three kingdoms.[14,15,16,17] Phytohormones are also critical for plants to adjust their development to ever changing environments and therefore link environment changes to bacterial and fungal growth. For example, manipulating hormone levels in the rhizosphere in response to an abiotic environmental change may sculpt roots to enhance specific microbial associations. Furthermore, most phytohormones impinge on plant immune systems, which can both hinder and help pathogenic and beneficial interactions.[14,18,19]

Microbes not only make phytohormones to manipulate plants but also directly respond to these small molecules.[12,20,21,22,23]. Unlike plants, however, we do not understand why or how these organisms perceive and transduce phytohormones into cellular responses. Partly, this is because most plant-associated microbes are not subjected to trait analysis that links genotype to phenotype because their genetics and biochemistry is complicated, and many are multinucleated. Also, many fungal interactions with plants are stochastic rather than functional, which clouds identifying true physiological interactions.

Fungi in soils predominantly belong to three phyla, Ascomycota, Basidiomycota and Mucoromycota (**Figure 1B**). Within Mucoromycota, studies on AM fungi of the Glomeromycotina clade dominate due to the importance these fungi play in nutrient exchange with plant roots.[24] AM fungal associations, which occur in over 80% of plant species are essential for plant growth and resilience to environmental stresses and are major drivers of agricultural productivity. Basidiomycota, which include mushrooms, often thrive as saprophytes living off wood and leaf litter (**Figure 1B**). For living plants, many Basiodiomycetes, such as rusts and smuts, are pathogenic.[25] Ascomycota, which descend from a common ancestor, are by far the largest and most diverse group of soil fungi encompassing plant pathogens, saprotrophs, and symbionts.[26]

The prevalence of Ascomycota in the rhizosphere suggested to us that the genetic model, *Saccharomyces cerevisiae* (yeast), which is also an Ascomycete, may have utility in understanding

plant-fungi associations. Yeast grows rapidly on defined media, possesses a well-annotated genome[27] and an abundance of mutational tools quickly connect phenotype to genotype.[28] Genome-wide knockout, haploinsufficient and overexpression collections, for example, are commonly used to identity small molecule protein targets.[29,30,31] Moreover, multigenic lines, forward genetic screens, and transformation facilitate elucidation of signaling mechanisms. However, laboratory yeasts are not favored in ecological and community studies, as strains are adapted to artificial environments that may genetically constrain their response to complex natural niches.[32,33,34]

At a granular level, evolutionary studies indicate that fungal regulatory networks are often rewired across species.[35] Yet, many features, such as polarized growth, adhesion, biofilm formation and drug resistance, are conserved across the fungal kingdom.[36,37,38] Indeed, yeast can naturally associate with plant material and laboratory strains can interact with plants.[32,39] Between 30 to 50% of Ascomycota species are estimated to associate with algae to form lichens[40] and astoundingly, yeast can also exchange nutrients with alga.[41] Although yeast is not filamentous, diploid yeast undergoes dimorphic growth or forms pseudohyphae under nutrient stress whilst haploid yeast can grow invasively into agar and even produce multicellular stalk-like structures under certain stress conditions.[42,43]

With this in mind, we developed a rapid integrative platform using yeast as an experimental system to identify fungal receptors and downstream effectors of plant-derived hormones. Elucidating the mechanisms of a hormone's action in yeast could then guide experiments in non-model fungi. Having no expectation whether plant small molecules would positively or negatively influence fungal growth, we used transcript profiling, rather than altered growth, to assess response to plant hormones. As a proof-of-principle, we demonstrated that two plant hormones induced distinct gene expression signatures in yeast. Focussing on one hormone, strigolactone (SL), we developed a pipeline consisting of mutational and structural analysis that identified the high-affinity Pi transporter, Pho84 as a putative SL target. This information directed experiments on two plant-associated fungi, an Ascomycete, and a Basidiomycete, which demonstrated that SL perturbs Pi homeostasis in both species. Our analysis indicated that yeast has utility in understanding the roles of plant hormones in plant-associated fungi and suggested this approach could be applied to other small molecule hormones. Furthermore, we believe the yeast platform developed here will be useful in characterizing the many plant-based natural products with respect

to fungal biology and should also work for molecules involved in other fungal-based interactions involving bacteria, insects, and worms.

RESULTS

SL elicits a transcriptional signature of Pi starvation in yeast

To determine whether yeast responds to plant hormones, we focused on the carotenoid-derived small molecule hormone, strigolactone (SL) (**Figure S1**). Although SLs regulate a number of developmental responses within plants including above ground branching and root architecture, they also emanate into the soil where they communicate to other organisms. Plant-derived SLs control densities and development within a population of plant species.[44,45] SLs also act as chemical signals used by parasitic plants to detect host plants, resulting in devastating yield losses in Africa.[46,47] With respect to fungi, the most studied response involves the symbiotic interactions between plants and Arbuscular Mycorrhizal (AM) fungi within the Mucuromycota phylum (**Figure 1B**).[22,48,49] When plants are low on Pi, they produce and exude more SLs that stimulate hyphal branching, which promotes plant-AM fungal connections.[22,23,24] These connections allow the transfer of inorganic phosphate (Pi) from the fungi in exchange for plant-derived carbon.[24] Finally, SLs appear to stimulate swarming of *Rhizobia* impacting root nodulation rates.[50] Thus, as a chemical cue in the soil, SLs are critical to organismal interactions across multiple kingdoms.

Because of the contributions of AM fungi to agricultural productivity and plant environmental resilience, these fungal species dominate SL studies.[51] SLs, however, not only influence AM fungi but also affect the development of a range of pathogenic Ascomycetes and Basidiomycetes.[21,52] Furthermore, soil microbiome studies indicate that genetically perturbing SL synthesis in plants affects the growth of several soil fungal taxa.[53,54] Although these observations suggest the fungal response to SL is broad, the differences in SL responses between studies question this conclusion.[55] To systematically survey the extent of SL response in fungi, we visually catalogued the response of 296 naturally occurring soil fungi to SL (**Figure 2, Figure S2, Table S1**).

Because of the prohibitive costs of natural SL synthesis, we used the synthetic SL, *rac*-GR24.[56] This artificial SL, which is commonly used for plant and fungal studies, is an enantiomeric mixture and therefore is not generally as potent as naturally occurring (+)-(2'*R*)-SLs found in nature (**Figure S1**). In the presence of low micromolar concentrations of *rac*-GR24, approximately

23% (67 Ascomycota, 2 Mucoromycota) of the fungi displayed visible responses to SL using eight criteria (**Figure 2, Figure S2, Table S1**). The high preponderance of Ascomycota species in the SL-responsive set suggested that yeast, which is also an Ascomycete, will respond to this hormone.

Since the application of *rac*-GR24 did not change the morphology of yeast, we performed RNA-seq experiments on SL-treated yeast cultures to determine if there is a transcriptional response. Addition of *rac*-GR24 to yeast resulted in a significant over-representation of genes annotated as involved in Pi acquisition (**Figure 3A, Table S2**). These included genes encoding secreted acid phosphatases (*PHO5, PHO11, PHO12*) that scavenge Pi from the environment, high-affinity Pi transporters (*PHO84*, *PHO89*) that increase Pi uptake efficiency, and vacuolar transporter chaperone complex subunits (*VTC1, VTC3*) that recycle Pi storage polymers (PolyP) (**Figure 3B**). We also detected an increase in *SPL2* expression, which encodes an inhibitor of the low-affinity Pi transporters, Pho87 and Pho90 (**Figure 3A, B**). The SL transcriptomic signature appeared similar to that of yeast cells starved for Pi. When yeast cells are depleted of Pi, they induce transcription of genes in the *PHO* regulon, which are involved in Pi homeostasis (**Figure 3C**).[57]

Although *rac*-GR24 caused changes in transcription, yeast growth on rich media was not perturbed suggesting there is compensation in response to altered Pi metabolism (**Figure S3**). Importantly, the specificity of gene expression pattern caused by SL can guide experiments to understand the mode of action of this hormone. We next show a methodology to turn SL-dependent transcriptome data into identification of a candidate target. We then demonstrate how target information can be expanded to other fungi through the development of new SL-related assays in two plant-associated fungi.

Strigolactone inhibits Pi uptake

The observation that SL perturbed Pi homeostasis in yeast is remarkable considering the importance of SL in facilitating plant-AM fungi symbioses, in which fungi provide Pi to the plant.[22,23,24] Fortunately, the molecular components involved in Pi acquisition in yeast are well characterized. Briefly, regulation of Pi-dependent gene expression depends on the nuclear localization of Pho4, a helix-loop-helix transcription factor.[58] In high Pi, a cyclin-dependent kinase complex (Pho80/Pho85) phosphorylates Pho4 excluding it from the nucleus. In low Pi, a decline in the inositol pyrophosphate 1,5-InP_8 releases the cyclin-dependent kinase (CDK) inhibitor,

Pho81, to inactivate the Pho80/Pho85 complex.[59] Consequently, unphosphorylated Pho4 accumulates in the nucleus where it interacts with a homeobox protein, Pho2, to activate transcription. Based on this model, we predicted that Pho4 will localize to the nucleus in the presence of *rac*-GR24 in cells grown in high Pi. Indeed, we detected accumulation of a *PHO4-YFP* translational fusion in the nucleus in the presence of *rac*-GR24 versus the mock control (**Figure 4A**).

Transcriptome and Pho4 localization data suggested that SL-treated yeast is starving for Pi and consistent with this, a 30-minute addition of *rac*-GR24 significantly reduced internal nucleotide phosphate and sugar phosphate pools, which are all hallmarks of Pi starvation (**Figure 4B, Table S3**).[60] Furthermore, yeast cells did not accumulate vacuolar polyphosphate (polyP) stores in the presence of *rac*-GR24 (**Figure 4C**).[61] When we directly monitored Pi acquisition by exposing yeast to a $^{32}PO_4$ tracer for ten minutes, there was a reduction in uptake of radiolabelled Pi in cells treated with *rac*-GR24 (**Figure 4D**). Furthermore, *rac*-GR24 addition reduced the rate at which yeast depleted Pi from the media (**Figure 4E**). Together, these data suggested that SL decreases Pi uptake in yeast resulting in Pi starvation and activation of the *PHO* regulon even in media replete with Pi.

Commonly used inhibitors of Pi transport normally work at millimolar concentrations in yeast and by contrast, *rac*-GR24 was approximately 200 times more potent, suggesting it has a unique mode of action.[62] With this said, the *rac*-GR24 concentrations we use were high (50 µM) compared to other SL-based experiments in fungi.[21,22] However, when we precisely measured the range of yeast response to *rac*-GR24 dose by monitoring acid phosphatase (AP) activity of a commonly used *PHO* reporter, Pho5,[63] we found that low micromolar *rac*-GR24 concentrations were sufficient to increase Pho5 activity (**Figure 4F**). Consistent with this, a transcriptional reporter, *PHO5pr-YFP*, also responded to 5 µM *rac*-GR24 dose (**Figure 4G**). Addition of the naturally configured (+)-(2'*R*)-GR24 isomer increased YFP signal at half the concentration (2.5 µM) of the racemic mixture (**Figure 4G**). Together, these results indicated that the SL response in yeast occurs within ranges commonly seen in other fungal and plant assays.[21]

Pho84 is a potential target of SL

In non-model systems, differentiating primary from secondary responses to a chemical are challenging. In yeast, however, primary and secondary responses can be separated by querying the

chemical response against collections of knockout mutants. Similar to placing genes in a pathway by genetic epistasis, perturbing proteins downstream of a chemical target usually reduce the ability to respond to that compound. The higher an insensitive mutant is in the pathway, the closer that gene is to the primary target. At the bottom of the pathway, *PHO5* expression is controlled by the transcription factors *PHO2* or *PHO4*. As expected, deletions of these genes abolished GR24-dependent AP activity, as did deletions of genes encoding Vip1 and Pho81, which inhibit the Pho80/Pho85 complex (**Figure 5A, Figure S4**). Notably, *rac*-GR24 did not induce AP activity when the high-affinity Pi transporter, Pho84, was deleted but did so in individual mutants deleted for the other Pi transporters, Pho87, Pho89, Pho90 (**Figure 5A, Figure S5**). The high placement of Pho84 in the Pi acquisition pathway, together with the ability of *rac*-GR24 to inhibit Pi uptake, suggested that SL inhibits Pho84 transport activity. Furthermore, loss of *PHO84* increases levels of the regulatory protein, Spl2, which further restrains Pi uptake through its negative regulation of low-affinity transporters.[64] Thus, *rac*-GR24 inhibition of Pho84 action should be suppressed by *spl2*Δ, and this was indeed the case (**Figure 5A, Figure S5)**.

Aside from mutant knockout analysis, three more lines of evidence suggested that Pho84 is targeted by SL. First, unlike other yeast Pi transporters, Pho84 is also a low-affinity transporter of manganese (Mn^{2+}) ions, and increased growth on inhibitory concentrations of Mn^{2+} is a good measure of reduced Pho84 activity.[65] With respect to Mn^{2+} sensitivity, *rac*-GR24 addition phenocopied a *pho84*Δ mutant showing reduced sensitivity to this heavy metal (**Figure 5B**). Second, overexpressing a target receptor candidate should result in hyposensitivity to the small molecule while decreasing dose of the target by half should result in hypersensitivity to the compound, causing haploinsufficiency.[30,31] As predicted, overexpression of *PHO84* decreased the ability of *rac*-GR24 to induce AP activity (**Figure 5C**) whilst deleting one copy of *PHO84* in a diploid caused a seven-fold increase in *rac*-GR24 responsiveness, as assayed by a *PHO5pr-YFP* reporter (**Figure 5D**). To eliminate the possibility that SL acts through the other Pi transporters, we used the yeast strain, EY917, which is deleted for all five Pi transporters (*pho84*Δ, *pho87*Δ, *pho89*Δ, *pho90*Δ, *pho91*Δ).[66] EY917 harbors a plasmid containing the *PHO84* gene under control of the *GAL1* promoter, making its Pi uptake and viability dependent solely on Pho84, which is only expressed on galactose.[66] The addition of *rac*-GR24 was sufficient to inhibit growth of EY917 on galactose (**Figure 5E**). In contrast, *rac*-GR24 did not inhibit growth of EY917 strains expressing either *PHO89* or *PHO90* (**Figure S5**).

Our genetic analysis suggests that Pho84 is a target of SL. However, biochemical analysis of Pho84 was challenging as it is a membrane-bound protein and SLs are hydrophobic. Therefore, we took advantage of strains expressing either *PHO89* or *PHO84* in tritiated *rac*-GR24 uptake experiments. Since the receptors are expressed inside the cells, any bound SL remains in the insoluble phase while unbound SL is present mostly in the soluble phase. We detected approximately 30% more radioactive signal in ethanol extracts from Pho84-expressing compared to Pho89-expressing yeast cells, indicating that SL preferentially partitions to cells containing Pho84 (Figure 5F). Next, we performed a drug affinity responsive target stability (DARTS) assay, which monitors protein stability as an output of ligand binding, on purified membrane fractions expressing HA-tagged Pho84.[67] We observed that the Pho84 protein was more resistant to protease digestion in the presence of *rac*-GR24. These results indicated that SL changes the conformation of Pho84 protein, making it more stable (Fig. 5F). These biochemical findings are consistent with our genetic analysis that Pho84 is an SL target.

If yeast Pho84 were an SL target, it should be possible to identify Pho84 mutants with reduced SL sensitivity without compromising Pi transport. To develop this screen, we again took advantage of the EY917 strain, which was transformed with a library of error-prone PCR (polymerase chain reaction)-mutagenized *PHO84*. Yeast that grows in the presence of *rac*-GR24 and glucose require that Pho84 does not recognize SL but remains functional for Pi transport (**Figure 6A**). Using these criteria, we identified two *PHO84* mutations, Ala262Pro and Gly256Asp, which when moved to the BY4742 strain, poorly induced AP activity in the presence of *rac*-GR24 (**Figure 6A**). When we mapped these two mutations onto a structure of the yeast Pho84 modeled on a highly related transporter from *Serendipita indica* (SiPT; PDB 7SP5)[68] as a template (**Figure 6C**), we identified a distinctive structural pocket at the lipid bilayer interface. Based on docking simulations, this pocket had a high fitness value binding likelihood for (+)-(2'*R*)-GR24 (**Figure 6D**). Ligand docking defined seven amino acids within the structural motif that could interact with GR24 and one of these, Gly256, was identified in our SL insensitive screen (**Figure 6D**). Importantly, the Asp substitution at position 256 was predicted to cause a clash with bound GR24 (**Figure 6C**). Using this structural information, we mutated other identified amino acids (Leu74, Ser212, Leu259) to the more hydrophobic and larger Phe and found that these substitutions also resulted in reduced GR24 sensitivity (**Figure 6E**). The clustering of these four single amino acid substitutions together with our modeling strongly suggested this structural

pocket defines a binding site for (+)-(2'*R*)-GR24 (**Figure 6E**). Consistent with this, structural modeling of the other three yeast Pi influx transporters that do not respond to SL did not reveal a structural pocket or conservation of amino acid sequence in the equivalent region of the protein (**Figure S5**). Finally, to further support the presence of a specific Pho84 SL binding pocket, we monitored Pho84 protein internalization from the plasma membrane. Pho84 internalizes to the vacuole in response to high Pi[69]. We discovered that addition of *rac*-GR24 internalized Pho84-GFP **(Fig. 6F).** By contrast, the addition of *rac*-GR24 did not internalize a mutant Pho84 receptor, which contains the L259F mutation on the predicted SL binding pocket and results in SL insensitivity **(Fig. 6F).** In summary, genetic, biochemical and cell biological data are all congruent with model that SL binds a binding pocket in yeast Pho84 protein, which inhibits Pi uptake and eventual internalizes this transporter from the plasma membrane.

Plant-associated fungi show SL-dependent Pi responses

The identification of Pho84 as a likely target of SL in yeast allows testing of this mechanism in non-model fungi. We did this using two plant-associated fungi, the beneficial symbiont, *Serendipita indica (Serendipita*) and the pathogen, *Fusarium graminearum* (*Fusarium*). *Serendipita* is a root basidiomycete that colonizes plants using intra- and intercellular hyphal networks both inside and on the root, resulting in improved Pi assimilation in a wide variety of plants.[70,71] As an endophytic Ascomycete, *Fusarium* causes head blight, a devastating disease for many monocotyledonous crops.[72] Both fungal species can grow axenically, reducing the experimental complexities inherent to obligate biotrophs.

As a test of the *in vivo* effects of SL on *Serendipita* and *Fusarium* we took advantage of the yeast-based Mn^{2+} inhibition assay.[65] As seen with yeast, *rac*-GR24 addition improved both *Serendipita* and *Fusarium* hyphal mat growth on inhibitory levels of Mn^{2+} compared to the mock control, a phenotype consistent with *rac*-GR24 inhibiting Pho84 transport (**Figure 7A, Figure 7B**).

Mn^{2+} resistance in both fungi was achieved at *rac*-GR24 levels five to ten times lower than those required in yeast experiments suggesting these plant-associated fungi are sensitized to this plant hormone. Addition of Mn^{2+} caused *Fusarium* to produce a reddish-orange pigment in response to *rac*-GR24 (**Figure 7A**). Aurofusarin, a reddish-orange pigment, is normally produced by *Fusarium* under Pi starvation.[73] Consistent with this, growing *Fusarium* on decreasing levels

of Pi increased pigment production (**Figure 7C**). We observed increased pigment production upon addition of low levels of *rac*-GR24 despite growing *Fusarium* on high Pi, suggesting that SLs induced a Pi-depletion response in this pathogenic Ascomycete. During early stages of plant infection, *Fusarium* produces aurofusarin, a response that is assumed to reflect the low Pi levels of the apoplastic space.[73] Our results suggest that aurofusarin production during plant infections may not be due to low apoplastic Pi levels but rather reflects exposure of *Fusarium* to plant SLs.

If SL treatment induces a Pi starvation response in *Serendipita* as it does in yeast, it should show an AP response. Mock-treated *S. indica* hyphal mats stained a light red color suggesting a low level of AP activity, and addition of low micromolar *rac*-GR24 measurably increased this activity (**Figure 7D**). Because AP assays can be performed in small volumes, we also tested AP activity using a natural, plant-derived SL, 5-deoxystrigol (5DS), and again detected increased AP activity on 1 µM 5DS (**Figure 7D**). Unfortunately, because *F. graminearum* produces aurofusarin in response to SL this precludes testing the ability of SL to induce AP activity.

SL, however, promotes hyphal branching of symbiotic fungi like AM fungi and phytopathogenic fungi.[22,23] Similarly, we observed that *rac*-GR24 increased hyphal branching, leading to a significant increase in spore production in *F. graminearum* (Figure 7E). To determine whether there is a direct functional connection between SL and *PHO84* in *Fusarium*, we knocked out *PHO84* in *F. graminearum* by CRISPR/Cas9 deletion methods. This *Fusarium PHO84* knockout line (ΔFGSG_07894) showed increased spore production versus wild type and this activity was insensitive to *rac*-GR24 addition **(Figure 7E).** In summary, SLs affect Pi-related responses in non-model fungi such as *Serendipita* and *Fusarium* and in the case of *Fusarium*, the SL-dependent increase in spore production requires a functional *Pho84*.

Conservation of SL binding pockets

The location of an SL binding pocket embedded in the lipid bilayer of the membrane is not unlikely as often the druggable sites of receptors, channels, and transporters occur at lipid-protein interfaces.[74] This suggests small molecules like SLs initially partition into the membrane before interacting with Pho84, which in turn, may affect efficacy. Whatever the case, the response of *Serendipita* and *Fusarium* to SLs in Pi-dependent assays led us to predict that Pho84 homologs in these fungi would contain similar transmembrane pockets. The *Serendipita* Pho84 crystal (SiPT; PDB 7SP5) showed a conserved pocket as did a modelled Pho84 structure from *Fusarium* (**Figure**

7F). To expand this analysis, we catalogued the seven amino acids that define the structural motif in Pho84 homologs from more than 1000 fungal species (**Figure 7G**).

Because amino acid composition is constrained by ligand binding, this analysis also probes patterns of binding site evolution. Ascomycota, for example, showed a preponderance of Phe at position 255 (blue block) compared to other phyla, but within this clade at position 74, the Saccharomycetales order is highly enriched for Met and Leu variation (yellow and green blocks) (**Figure 7G**). By contrast, position 256 dominates with a conserved Gly (grey block) but a section of Ser (orange block) defines a Basidiomycota clade that includes *Serendipita* (**Figure 7G**). Although the consequences of these phylogenetic differences are unclear, plants make different types and amounts of SLs,[75] so perhaps these differences translate to different plant associations. Finally, position 259 contains an invariant Pro (ruddy pink block) except for the S. *cerevisiae* S288c laboratory strain, which contains a Leu in this position (**Figure 7G**). Interestingly, swapping this Leu for a Pro decreases sensitivity to polychlorinated fungicides[76] and we find substituting a Phe at this position results in decreased *rac*-GR24 sensitivity. Pro and Phe kink transmembrane helices, which may decrease small molecule binding in this region. Notably, the Ala262Pro mutation identified in our SL-insensitive screen is a substitution on the same transmembrane helix.

Methyl jasmonate also causes specific transcriptional signature in yeast

The specificity of yeast transcription upon SL addition indicated that this model Ascomycete can respond to a plant hormone. However, it is possible this response is limited to SL and that other plant hormones will not cause unique transcriptional signatures. To test this, we tested the ability of yeast to respond to another structurally unrelated plant hormone, Methyl Jasomonate (MeJA). Jasmonates represent a class of oxylipins including Jasmonic Acid (JA), its precursor 12-Oxo-PhytoDienoic Acid (12-OPDA), and JA derivatives such as Methyl Jasmonate (MeJA) and JA-Isoleucine (JA-Ile).[77] Jasmonates are made when plants are wounded or during pathogen infections particularly those involving necrotrophic fungal pathogens.[78,79] Furthermore, the volatile nature of MeJA allows this jasmonate to act as a long-distance communication signal between plants. Surprisingly, although jasmonates are plant protectants, fungi also produce them, often in large amounts.[80] MeJA inhibits hyphal growth of post-harvest fungal pathogens[81] and proteomic analysis of the medically important basidiomycete, *Ganoderma lucidum*, shows that MeJA affects protein levels in multiple processes.[82] Interestingly, fungi also respond to other related oxylipins,

some of which are implicated in quorum sensing.[83,84] Based on a literature survey, numerous Ascomycetes and Basidiomycetes respond to MeJa (**Figure S6**).

MeJA application on yeast also caused changes in gene expression, but unlike SL, these were not related to Pi homeostasis (**Figure S6, Table S2**). For example, genes involved in alternative carbon metabolism such as the glyoxylate cycle (*ICL1, IDP2, CIT2, MDH2, MLS1*), gluconeogenesis (*FBP1, FBP25, PCK1*), sucrose transport (*SUC2*), galactose (*GAL1, GAL2, GAL7*), glycerol (*STL1, GUT1, GUT2*) and glycogen (*GDB1*) catabolism were up-regulated whilst primary glucose metabolism genes (*HXT2, HXT3, HXT4, HXK2*) were down-regulated (**Figure S6, Table S2**). We also detected down-regulation of genes involved in translation (**Figure S6, Table S2**). These expression patterns which are characteristic of yeast growing on glucose-depleted media, were surprising as yeast cultures were grown on rich media containing glucose and we did not detect any decrease in growth rates (**Figure S3**). Normally, yeast does not utilize alternate carbon sources until glucose is consumed.[85] A MeJA connection to yeast sugar metabolism, however, is intriguing since this hormone also appears to down-regulate glucose metabolism in *Ganoderma*.[82] In summary, yeast shows a specific transcriptional response to exogenous MeJA but like SL, MeJA did not appear to affect yeast growth on rich media. The response of yeast to MeJA appeared to involve genes involved in sugar metabolism.

DISCUSSION

An approach to decoding plant small molecule inter-kingdom signals

Identifying plant compounds that communicate across kingdoms is challenging because of a lack of robust assay systems to query the vast numbers of secondary products produced by plants. In this study, we present a straightforward approach centered around the model, *Saccharomyces cerevisiae* to systematically identify and decipher plant-derived small molecules that communicate with fungi. Key to our approach was the use of transcript profiling as a chemical output. Gene expression is a highly sensitive chemotyping tool and importantly, this technique captures the phenotypic output caused by the chemical input independently of whether the compounds affect growth. For example, although both SL and MeJA induced specific expression profiles, they did not appear to impact yeast growth or morphology on rich media. Moreover, by monitoring global transcriptional patterns rather than changes in expression of a few genes, modes-of-action can be more confidently hypothesized. For instance, expression patterns of both SL- and MeJA-treated

yeast clearly pointed to perturbations in Pi and sugar metabolism, respectively. In the case of SL, our investigation led to the identification of a potential target, the high-affinity Pi influx transporter, Pho84.

A number of plant-associated fungi models do exist but because they mostly encompass plant pathogens, research is mostly tailored to identify genes related to pathogenesis.[86] By contrast, models to interrogate inter-kingdom communication between plants and fungi have not been developed. As an alternative to developing a new system, yeast allows fungal researchers to tap into the vast genetic resources of this Ascomycete. Mutant libraries can map the action of compounds to regulators of specific pathways and forward genetics can quickly identify potential targets. Multigenic strains and reporter constructs simplify genetic redundancy issues that would be challenging in other fungi. Finally, yeast mutational analysis interfaces well with structural modeling and, in principle, with the advent of AI-based programs, any yeast protein can be modelled. SL-insensitive mutants identified a Pho84 structural pocket required for SL action and combined with *in silico* ligand binding analysis, this information predicted which fungal species could respond to this plant hormone without experimentation. Notably, *Fusarium* and *Serendipita,* which also contain a Pho84 pocket, both showed Pi-related phenotypes such as increased Mn^{2+} resistance in the presence of SL.

The fact that fungi from two different phyla responded in a similar manner to SL suggests that these perception mechanisms are most likely conserved across the fungal kingdom.[87] Our success with SL and MeJA applications suggest that other plant growth regulators will also produce specific transcriptional signatures, revealing the process targeted by the small molecule. Addition of ABA to *Aspergillus*, for example, results in differential expression of over 15,000 genes, whose functions have been annotated to a variety of categories.[88] An ABA target was not identified likely because many processes were affected, perhaps reflecting the complexity of the *Aspergillus* lifecycle. On this note, the developmental simplicity of yeast may result in a more precise ABA-dependent transcript profile. Importantly, mutational analysis can be applied to identify hormone-insensitive yeast mutants as was our strategy in identifying *PHO84*. In conclusion, it appears yeast is a good model to study inter-kingdom chemical communication between plants and fungi.

Roles of SL in the rhizosphere

The identification of Pho84 as a fungal SL target raises questions about both the origin and function of this phytohormone in the rhizosphere. When plants first colonized land approximately 400 million years ago, they faced a major challenge in acquiring nutrients such as Pi from the soil.[89] To efficiently acquire nutrients, plants are hypothesized to have recruited saprophytic or weakly pathogenic fungi.[90] In this context, SLs most likely acted as defensive chemicals keeping fungal partners in check. Over time, as plants dampened fungal pathogenesis, mutualistic associations could evolve SL into a beneficial external signal. This blurring of pathogenesis and mutualism through shared components is common to plant-fungal interactions.[90] Inhibition of fungal Pi homeostasis, for example, could explain how SLs act as allelopathic compounds in soil. Decreasing Pi uptake would compromise invasive fungal growth, an action consistent with the increased pathogen susceptibility of SL-deficient plants.[55]

For fungal mutualists on the outside of the root, SL inhibition of Pho84 could encourage these ectophytes to secrete AP, increasing plant accessibility to soluble Pi in the soil. **Moreover, SL could mimic a phosphate starvation response in the fungus by inhibiting Pho84, which encourages germinating hyphae to grow towards a plant in search of phosphate. Additional roles of SL on hyphal growth inside plant cells is complicated as measuring internal SL concentrations in specific tissues or individual cell types is challenging. If, however, SL were to mediate plant-fungal interactions inside the plant, one could envision a scenario where SL enhances the net flux of phosphate from the fungus to the plant cell.** Although arbuscules allow Pi to be directly effluxed to the plant cell, in principle, fungi could also reabsorb this Pi through Pho84. In this context, inhibition of fungal Pho84 by plant SL would facilitate a unidirectional flow of Pi from the fungus to the plant cell, which may explain why SL is required for activation of AM fungi in the rhizosphere and their attachment to the root.[48] Whatever the case, our observations that yeast Pho84 function and Pi homeostasis are also regulated by SL posit mechanisms that would be difficult to discern from AM fungi. An AM fungus called *Rhizophagus irregularis* for example, has three full-length Pho84 homologs[91] but only two possess a SL transmembrane binding site based on modeling (**Figure S7**). These observations predict that AM fungi contains both SL-regulated and SL-independent high affinity Pi transporters, which further demonstrates the complexities of this system.

Many fungi synthesize different plant hormones, and it is generally thought this is to manipulate the lifestyle of the plant.[7,12] It is also possible that fungi produce plant hormones for its

own growth and plants exude hormones into the soil to hijack functions in fungi. This latter model would explain why fungi not associated with plants respond to the hormone auxin.[92,93] In this scenario, fungi may make an SL-like molecule (fungal-SL) under certain physiological conditions such as high Pi to down regulate its own Pi uptake. Although no SL-like molecules have been identified in yeast, amino acid substitutions in the Pho84 transmembrane SL binding site alter responsiveness of yeast to particular fungicides suggesting this pocket does bind other small molecules.[76] At any rate, molecular genetic tools in yeast should facilitate identification of fungal-SL and its roles in fungal physiology, which again highlights the importance of a yeast model.

Limitations of the study

For half a billion years, plants and fungi have coordinated their association through a language which includes small molecules. Our methodology used yeast to query how plant hormones elicit responses in fungi based on the assumption that yeast has similar response pathways to other fungi. Academic arguments for why laboratory yeast is not a good system for "real-world" fungi permeate the literature, so we were surprised that the first two plant molecules we chose, SL and MeJA, both elicited precise and specific transcriptional responses. We do not believe the similarities in the nutrient-small molecule connection are due to chance, and we predict that other plant hormones will also generate clear transcriptional patterns that relate to plant processes. Unfortunately, quickly testing the information gleaned from our yeast pipeline in non-model fungi is not easy due to the experimental challenges associated with these species. Mostly, these involve normalizing biochemical and molecular experiments using filamentous mats versus yeast-like colony growth. By definition, interkingdom studies rely on the presence of a host further complicating experimental designs. Finally, it is difficult to compare our experimental results to physiological conditions and concentrations of small molecules both within and outside of plants. We saw responses in yeast at the low micromolar range and many fungi in petri plate assays respond at this concentration.[22] SLs, however, are suggested to be at nanomolar SL concentrations based on measurements of hydroponic solutions surrounding growing plants so within and around the roots this hormone must be markedly higher.[94] Furthermore, many fungi, including the *Fusarium* sp. and *Serendipita* sp., used in this study, form intimate connections within plant roots, where hormone levels will be higher than those found in the soil. Hormones also must accumulate to higher levels in particular regions of the root, possibly in response to fungal symbionts. Without

more quantification of hormone levels within plant roots and in the soil around plants, it is difficult to position our small molecule experimental designs in a context of natural levels of hormones either in the soil or within plants. **AM fungal hyphae, for example, respond to nanomolar ranges of SLs, which is orders of magnitude less than the response we see in yeast.[23,24] Perhaps the SL signal in hyphae of AM fungi does not go through Pho84 but rather, through a different response system. Alternatively, Pho84-dependent signaling in AM fungi may be highly sensitized to SL compared to yeast.**

Although the effect of SL in perturbing Pi homeostasis appeared to be conserved in yeast, *Serendipita*, and *Fusarium*, there are limitations to our approach based on the extent of pathway conservation and absence of various developmental stages in lab yeast. First, although SL response requires PHO84, it may not formally be a receptor that transduces this hormone signal. Possibly SL is a specific inhibitor of this Pi transporter. Relating to this, the roles of Pho84 in yeast are complicated as this transporter is reported to have both transport and signaling functions.[62] If SL is an inhibitor of Pho84 function, it appears its mode of action is fundamentally different to identified Pi transport inhibitors which require orders of magnitude higher concentrations to work.[62] The sensitivity of SL inhibition on Pho84 may reflect its mode of action, which appears to be allosteric rather than orthosteric like other Pi transport inhibitors. Whatever the case, more detailed biochemical analysis, particularly showing direct binding of SL to Pho84, is required to fully understand SL action on this transporter.

Second, although Pho84, is highly conserved in the fungal kingdom, it is possible that targets of other small molecules like plant hormones are not conserved. There could also be multiple targets affected by a single molecule, which are not present in lab yeast. Third, although core components of signalling pathways are often conserved in fungi, pathways may have been rewired and/or consist of different components.[37] For example, the roles of InP isomers which function as secondary signals in Pi homeostasis, appear to have flipped in *Cryptococcus neoformans* in comparison to yeast.[95] Finally, small molecules could perturb processes at developmental stages that lab yeast do not undergo, such as dimorphic growth. In this scenario, we will not detect responses to the compound using lab yeast. All these factors could also cloud validation of the effects of these compounds in other fungi.

The inability of lab yeast to switch to filamentous growth may be key to detecting precise and specific transcript profiles. Perhaps the reason that hormones like SL and MeJA induce diverse

transcriptional changes in filamentous fungi is that these fungi can proceed through different developmental stages. Transcript profiles reflect the cascade of the signalling pathways affected by the small molecule. While complexities of ‘real world’ fungi could complicate extrapolation of the mechanisms of these signals, our pipeline demonstrated the utility of budding yeast as a model for fungal responses to small molecules as an essential starting point.

Acknowledgments:

We would like to thank Dr. C. Boone for yeast strains, experimental advice, and thoughtful comments throughout the study.

Funding: This research was supported in part by Digital Research Alliance of Canada (https://alliancecan.ca/en). MB was partially funded by a Natural Sciences and Engineering Research Council of Canada (NSERC) predoctoral fellowship. This work was supported by a NSERC Discovery Grant (no. 06752), an NSERC Accelerator Supplement (no. 507992), an NSERC Research Tools and Instruments grant (no. 00356), a New Frontiers in Research Fund (NFRFE-2018-00118) and a France-Canada Research Fund awarded to SL as well as an NSERC Discovery Grant (no. 04298) awarded to PM.

Author contributions: Conceptualization, S.L. and P.M.; Methodology, S.L., P.M., J.M.B., M.B., and D.H-S; Investigation, J.M.B., M.B., F.Z.W., G.L., B.A., D.H-S., Y.T., S.S., N.K., and R.O.; Writing-original draft, S.L., and P.M.; Writing-Review & Editing, J.M.B., M.B., F.Z.W., B.A., G.L., and Y.T.; Data curation, G.L.; Visualization, G.L., S.L., P.M., J.M.B., M.B., and B.A.; Project Administration, S.L.; Funding Acquisition, S.L., P.M.; Resources, F-D.B., and C.S.P.M.; Supervision, S.L., P.M., and Y.T.

Competing interests: The authors report no potential competing interests.

Data and materials availability: All yeast strains created in this study are available upon request. Raw fastq sequence files for transcriptome profiling of *rac*-GR24-treated yeast cells are available as a Sequence Read Archive (SRA) with the BioProjectID: PRJNA966945. Processed differential expression values are available in Table S1. Raw flow injection mass spectrometry data is available under dataset identifier MTBLS7371 within the Metabolights database (https://www.ebi.ac.uk/metabolights). Processed flow injection mass spectrometry data is available in **Table S3**. All data are available in the main text or the supplementary materials.

Figure Title and Legends

Figure 1. Yeast as a model for interkingdom signaling

(**A**) Chemical structures of the major plant hormones.
(**B**) Cladogram of fungal kingdom.[88] *Saccharomyces cerevisiae* (yeast) is identified with a red box. Arrows and circles denote significant innovations of evolution along the fungal lineage. Triangles denote the evolution of mycorrhizae along the lineage.
(**C**) Integrative pipeline to identify fungal processes affected by a plant hormone. The initial step is transcript profiling of yeast treated with a small molecule. Upon identification of the process affected by the compound, genetic and genomic tools in yeast pinpoint signalling components. This information guides structural analysis to identify potential targets. Structure-function analyses can inform mutational analysis of a target. Once a process is identified, assays can be developed involving real-world plant-associated fungi.

Figure 2. Response of soil fungal species to SL

(**A**) NCBI common tree of the Ascomycota and Mucoromycota phyla that respond to SL. Colored heatmap denotes which clades exhibited physiological effect(s) from the 1 µM *rac*-GR24 treatment.
(**B**) Representative images of each visual category across a collection of fungal species from Figure 2A. For a complete set of strain lists, data, and images, see **Table S1 and Figure S2**.

Figure 3. SL elicits transcriptional signature of phosphate starvation in yeast

(**A**) SL-induced gene expression. Volcano plot representation of differentially expressed genes in 50 µM *rac*-GR24-treated relative to DMSO-treated yeast. Dotted lines represent ≥2 and ≤2-fold changes in gene expression. Labelled red dots depict *PHO*-related genes (**Table S2**).
(**B**) Placement of SL-regulated genes into the phosphate starvation (*PHO*) regulon. Low phosphate levels activate transcription of *PHO* regulon genes (blue arrows). Red arrows represent *rac*-GR24-induced genes.
(**C**) Left, over-representation of *rac*-GR24-induced genes related to phosphate metabolism by GO annotation (**Table S2**). Right, changes in expression levels of genes induced by *rac*-GR24 in comparison to their induction under low phosphate.

Figure 4. SL inhibits Pi uptake

(**A**) Representative images of *Pho4-eYFP* cellular localization after 2 h treatment with or without 50 µM *rac*-GR24. White arrows, nuclei.
(**B**) Metabolome profiling of yeast treated with 50 µM *rac*-GR24 for 0.5 h. Heatmap shows $\log_2$-fold changes.
(**C**) PolyP accumulation on 50 µM *rac*-GR24. Numbers represent relative intensities after 4 h of treatment relative to the zero timepoint. PPstd, PolyP standard.
(**D**) *rac*-GR24 inhibition of Pi uptake. Wild type BY4742 strain exposed to ^{32}P for 10 min. Uptake was measured by radioactive accumulation. *** p-value < 0.001.
(**E**) Supernatants measured for Pi concentrations using a molybdenum blue method (see **Methods**). *** p-value < 0.001. All experiments were performed using 50 µM *rac*-GR24.
(**F**) Sensitivity of yeast to *rac*-GR24. Response to SL was monitored by following a secreted acid phosphatase (AP) activity that can be assayed using a colorimetric stain where increased

activity results in redder colonies.[63] BY4742 yeast were spotted onto 5 mM Pi stained for AP activity (red).
(**G**) *PHO5pr-YFP* reporter expression. The BY4742 strain was grown in 0.5 mM Pi with increasing concentrations of *rac*-GR24 or the (+)-(2'*R*)-GR24 isomer for 10 h. *PHO5pr* expression was normalized to OD_{600}. Significance of (+)-(2'R)-GR24 relative to DMSO control was assessed by two sample t-test. ** p-value < 0.005. *** p-value < 0.0001.

Figure 5. *PHO84* is required for SL induction
(**A**) Acid phosphatase (AP) activity of *PHO* regulon deletion (Δ) strains in the presence of 50 μM *rac*-GR24 on 5 mM Pi. Represented here is an abbreviated version of the yeast *PHO* regulon. Pi can enter the cell through multiple Pi transporters (low affinity Pho87, Pho90, high affinity Pho89, Pho84). Inside the cell Pi can be converted to inositol phosphate intermediates (InP) and/or transported to the vacuole through the VTC complex. Vacuolar Pi forms Poly Phosphates (PolyP) which can be metabolized back to Pi and exported though Pho91 into the cytoplasm under Pi stress. In low Pi, a decline in the inositol pyrophosphate 1,5-InP8 releases the cyclin-dependent kinase (CDK) inhibitor, Pho81, to inactivate the Pho80/Pho85 complex. Phosphorylation of Pho4 by Pho85 excludes this transcriptional activator from the nucleus under Pi replete conditions. Relative intensities of AP staining (red) on *rac*-GR24 relative to mock treatment were quantified (**Figure S4)**.
(**B**) Manganese (Mn^{2+}) sensitivity of yeast on SL. Top row, representative image of the growth of wild type yeast (BY4742) on media containing 8 mM $MnCl_2$ ± *rac*-GR24. Lower row, representative picture of the growth of *pho84*Δ deletion line ± 50 μM *rac*-GR24.
(**C**) Overexpression (o/e) of *Pho84* in yeast results in hyposensitivity to 50 μM *rac*-GR24 as measured by AP activity.
(**D**) SL-induced haploinsufficiency in yeast. Reduction of *Pho84* gene dose by half (*pho84*Δ/+) results in a seven-fold increase in sensitivity to 50 μM *rac*-GR24 based on expression of *PHO5pr-YFP* relative to culture density (OD_{600}) in yeast.
(**E**) Synthetic lethality in a *PHO84*-expressing strain on *rac*-GR24. EY57 is a wild-type strain containing all functional transporters. EY917 is deleted for five *PHO* transporters and is expressing *PHO84* from a *Gal1* promoter.
(**F**) Top panel, SL preferentially binds Pho84-expressing yeast cells. Yeast cells expressing either *PHO89* or *PHO84* only were incubated with 1 μM H^3-*rac*-GR24 and then counted for radioactivity. ** p-value < 0.005 Bottom panel, Pho84 protein is preferentially protected from degradation in the presence of SL using a drug affinity responsive target stability (DARTS) assay. Yeast membranes expressing a His-tagged Pho84 were incubated with 50 μM *rac*-GR24 and subsequently treated with a range of pronase concentrations. Pho84 was detected by PAGE immunoblotting.

Figure 6. **Pho84 contains a transmembrane binding pocket required for SL response**
(**A**) Left, EY917 expressing either a *pho84-G256D* or a *pho84-A262P* mutation. Right, BY4742 strains expressing either a *pho84-G256D* or a *pho84-A262P* mutation stained for AP activity.
(**B**) Phosphate uptake in wild type *PHO84*, *pho84-G256D* and *pho84-A262P* lines in the presence and absence of 50 μM rac-GR24.
(**C**) Structure of the yeast Pho84 protein modelled on an occluded *Serendipida indica* high-affinity phosphate transporter (PDB 7SP5). Enlargement, pocket domain with two mutant

amino acid substitutions (*pho84-G256D*, *pho84-A262P*). The Gly256Asp substitution clashes with a docked (+)-(*2'R*)-GR24 isomer (cyan sticks).
(**D**) Left panel, Interactions between Pho84 binding pocket residues (green sticks) and a (+)-(*2'R*)-GR24 isomer (blue sticks). Right panel, Red fans indicate potential hydrophobic contacts.
(**E**) Analysis of mutations in SL binding pocket in Pho84. Position of Pho84 amino acid residues, AA74, 212 and 259 are represented by yellow spheres. AA256 is represented by a red sphere. Cyan sticks represent docked (+)-(*2'R*)-GR24 isomer. Growth of EY917 expressing either *pho84-L74F*, *pho84-S212F*, or *pho84-L259F* on 100 µM *rac*-GR24.
(**F**) Pho84 localization in response to SL. A line carrying the wild type *PHO84*-GFP or the *pho84-L259F*-GFP allele are imaged before and after a two-hour 50 µM *rac*-GR24 incubation. Arrows, white: plasma membrane, yellow: vacuole.

Figure 7. Plant-associated fungi respond to SL
(A) Manganese (Mn^{2+}) sensitivity of *Fusarium graminearum* (*Fusarium*) on synthetic media containing 10 mM $MnCl_2$ in the presence or absence of 10 µM *rac*-GR24. Plates were photographed from above (top panels) and below (bottom panels).
(**B**) Mn^{2+} sensitivity of *Serendipita indica* (*Serendipita*) on synthetic media containing 0.75 mM $MnCl_2$ in the presence or absence of 5 µM *rac*-GR24. Growth was quantified for $MnCl_2$-treated cultures (n=8) by measuring fungal area (cm^2). Scale represents 1 cm. Cultures grown on 5 µM *rac*-GR24 had significantly greater colony areas, *** p-value < 0.001.
(**C**) Growth of *Fusarium* on synthetic media in the presence or absence of 5 µM *rac*-GR24 on increasing levels of Pi.
(**D**) Acid phosphatase activity of homogenised *Serendipita* cultures spotted onto synthetic media containing 1 mM Pi and supplemented with 5 µM *rac*-GR24 or 1 µM of a naturally occurring SL, 5-deoxystrigol. Increased red staining indicates higher AP activity. Intensities of red staining on SL relative to mock (DMSO) treatment were quantified in the graph below.
(E) SL works through Pho84 to regulate hyphal branching and spore formation in *Fusarium*. Left panel, a representative image of *Fusarium* hyphae in the presence or absence of 15 µM *rac*-GR24 3h post-inoculation. Right panel, quantification of spore production of a wild type *PHO84* and mutant *pho84* knockout line in the presence or absence of *rac*-GR24. ** p-value < 0.01, *** p-value < 0.001, N.S not significant.
(**F**) Structural models of *Serendipita* (SiPho84) and *Fusarium* (FgPho84) Pho84. Red, key amino acids involved in SL recognition.
(**G**) Proportion of amino acids in the SL binding motif at each position in Pho84 sequences from the fungal kingdom. Arrow, *Saccharomyces cerevisiae* laboratory strain (S288c). Black lines indicate that gene could not be identified.

STAR METHODS

RESOURCE AVAILABILITY

Lead Contact

Further information and requests for resources and reagents should be directed to and will be fulfilled by the lead contact, Shelley Lumba (shelley.lumba@utoronto.ca).

Materials availability

All strains and constructs generated in this study are available upon request from the lead author.

Data and code availability

Raw RNA sequence data for transcriptome profiling of GR24-treated and MeJA-treated yeast have been deposited at National Center for Biotechnology Information (NCBI). Raw flow injection mass spectrometry data have been deposited at the Metabolights database (https://www.ebi.ac.uk/metabolights). Data are publicly available as of the date of publication. Accession numbers are listed in the key resources table. Any additional information required to reanalyse the data reported in this paper is available from the lead contact upon request.

EXPERIMENTAL MODEL AND STUDY PARTICIPANT DETAILS

Saccharomyces cerevisiae strains

Table S4 lists all *Saccharomyces cerevisiae* (henceforth: yeast) strains and plasmids used in this study. Overexpression plasmids for key genes in the phosphate starvation pathway were gifted by Dr. Charles Boone (**Table S4**). Knockout strains were purchased from Transomic Technologies^{Ltd}, except for *pho84*Δ and *pho80*Δ, which were made according to standard laboratory procedures using homologous recombination to replace the open reading frame with a KANMX gene conferring resistance to geneticin. To construct the *BY4743 pho84*Δ/+ strain, BY4742 *MATα pho84*Δ was crossed with BY4741 *MATa wildtype* and diploids selected on synthetic media lacking lysine and methionine.

Filamentous fungal strains

The *Serendipita indica* strain was purchased from ATCC with the strain designation END1 [DSM 11827] (product code: 204458). *Fusarium graminearum* (strain ID: DAOM 233423) was kindly gifted by Dr. Rajagopal Subramaniam.

METHOD DETAILS

***Saccharomyces cerevisiae* growth conditions and transformation**

S. cerevisiae was incubated at 30˚C with shaking at ~225 rpm when grown in liquid media. Unless otherwise stated, experiments were conducted in either Yeast Peptone Dextrose (YPD) or Yeast Nitrogen Base (YNB) without amino acids and without phosphate. For YPD, 12.5 g peptone and 6.25 g yeast extract were dissolved in 1 L dH_20 and autoclaved. For the YNB, amino acids were supplied with the appropriate dropout, depending on genotype.[114] Unless otherwise stated in figure legend, 2 % glucose was used as the sole carbon source. Inorganic phosphate (Pi) was supplied as KH_2PO_4 to a final concentration of 0.05, 0.5, 5 or 10 mM (as described in figure legend), and potassium levels were adjusted to 10 mM using KCl. For solid media, agar was added prior to autoclaving to a final concentration of 2 % (w/v).

In all cases, yeast was transformed using a standard lithium acetate approach.[96] Briefly, an overnight yeast culture was back diluted to OD_{600} ~ 0.4 in a volume of 40 ml and grown at 30˚C for ~ 4 h. Cells were pelleted, washed twice in dH_2O and resuspended in 400 µl 0.1 M sterile lithium acetate. For each transformation, 50 µl of cells were pelleted and resuspended in 34 µl dH_2O containing the recombinant DNA fragment or plasmid to transform into yeast. Typically, a total of 400 ng – 800 ng of DNA / plasmid was used per transformation. The following transformation mix was then added to the cell suspension and mixed by pipetting: 240 µl 50 % PEG 3350 (autoclaved), 36 µl 1 M lithium acetate (autoclaved) and 50 µl 2 mg.ml salmon sperm DNA (boiled for 5 min and cooled on ice for 2 min). Cells were incubated at 30˚C for 25 min, then at 42˚C for 25 min. Cells were pelleted and resuspended in 1 ml dH_2O. Typically 100 µl cell suspension was spread onto a Petri dish and these were incubated at 30˚C for 2-3 d to recover transformants.

Plasmid construction

For construction of the *PHO5* promoter (*PHO5pr*)–yellow fluorescent protein (*YFP*) transcriptional fusion (*PHO5pr-YFP*), the *pAG415GAL-ccdB-YFP* backbone carrying the *LEU2* selectable marker[97] was modified by PCR-directed deletion of the *GAL1* promoter using primers: remove-GAL1-SacI-F and remove-GAL1-SacI-R (**Table S5**). The resulting PCR product was digested with SacI and ligated with T4 ligase, according to the manufacturer's instructions, and named *pAG415m-ccdB-YFP*. Then, a 1,000 bp region upstream of the *PHO5* open reading frame was amplified from genomic DNA extracted from the BY4742 yeast strain with primers containing Gateway-compatible overhangs. The primers (*PHO5pr-attB1* and *PHO5pr-attB2*) contained partial Gateway®-compatible overhangs to add the *attB* sites (**Table S5**). The full *attB* sites were added by a second round of PCR using a generic primer pair: generic-GW-*attB1* and generic-GW-*attB2* (**Table S5**) and the PCR product cloned into pDONR221 and subsequently into *pAG415m-ccdB-YFP* via BP and LR reactions, respectively.

For construction of the *PHO4-YFP* translational fusion, the *PHO4* coding sequence was amplified from *BY4742* genomic DNA using primers (pho4-attB1 and pho4-attB2) that lacked the stop codon, and which included Gateway®-compatible overhangs (**Table S5**). The PCR product was cloned into *pAG415m-ccdB-YFP* as described above for the *PHO5pr*. The resulting *PHO4-YFP* fusion was amplified from the plasmid using a forward primer (pAG415-PHO4CDS-up) that bound upstream of the coding sequence in the plasmid backbone and a reverse primer (PHO4-YFP-Int-R) that annealed to the *LEU2* selectable marker, and which included additional sequence that was homologous to a region downstream of the *PHO4* genomic locus (**Table S5**). Another round of PCR using a second reverse primer (PHO4-YFP-Int-R-OH) was used to add further homology downstream of the *PHO4* genomic locus (**Table S5**). The resulting PCR fragment was transformed into BY4742 and integration events selected on media lacking leucine. The integration at the native locus was confirmed by PCR and by nuclear localisation of *YFP* under low Pi conditions.

A plasmid suitable for PCR-directed mutagenesis of *PHO84* (called *pAG413m-PHO84pro-PHO84*) was made in the following way. First, the pAG413 backbone was amplified using primers, Pi-pAG413-MCS-F and pAG413-MCS-R (**Table S5**). Second, a LacZa fragment containing a multiple cloning site (MCS) from pUC19 was amplified using primers, Pi-pUC19-LacZa-F and pUC19-LacZa-R (**Table S5**). The forward primers had a phosphorylated 5' end to allow blunt end ligation via T4 ligase to yield the plasmid, pAG413-LacZa-MCS. The *PHO84*

promoter and coding region (*PHO84pro-PHO84*) was amplified from BY4742 genomic DNA using primers, PHO84p-BamHI-F and PHO84-cds-SacI-R which included SacI or BamHI restriction sites (**Table S5**). The *PHO84pro-PHO84* PCR fragment and the pAG413-LacZa-MCS plasmid were double digested with BamHI and SacI and then ligated with T4 ligase to generate *pAG413m-PHO84pro-PHO84*, which was used as the template for random mutagenesis of *PHO84* (see below section entitled *PHO84* PCR mutagenesis and GR24 insensitive screen).

The two mutant strains shown in Fig. 6A (*pho84*-G256D and *pho84*-A262P) were constructed by gap-repair cloning in the EY917 background (described below). The constructs were amplified using a forward primer annealing to the *PHO84* promoter (PHO84pr-Int-F) and a reverse primer against the *LEU2* selection marker (PHO84-Int-LEU-R) (**Table S5**), and integrated at the native locus (as described for *PHO4-YFP*) to yield the following strains: BY4742 *PHO84::ScPHO84* (wildtype control), *PHO84::Scpho84-G256D* and BY4742 *PHO84::Scpho84-A262P* (**Table S4**). The presence of the mutations in transformants was confirmed by Sanger sequencing.

The *PHO84-GFP* strain (**Table S4**) was constructed by first amplifying *PHO84* CDS from genomic DNA using primers PHO84-attB1-F and PHO84-attB2-R with Gateway®-compatible overhangs (**Table S5**). The PCR product was cloned into *pAG415GAL-ccdB-EGFP*[97], as described for *PHO5pr*. The *PHO84-EGFP* region was amplified using a F primer that bound to the start of the CDS (PHO84-CDS-F) and a reverse primer (Pho84-leu2-Int-R) that annealed to the *LEU2* selectable marker in the plasmid backbone, and which included sequence homology to a region downstream of the *PHO84* genomic locus (**Table S5**). Another round of PCR using a second reverse primer was used to add further homology downstream of the *PHO84* genomic locus (Pho84-leu2-Int-R-OH) (**Table S5**). The resulting PCR fragment was transformed into BY4742 and integration events selected on media lacking leucine. The integration at the native locus was confirmed by PCR and by induction of *PHO84-EGFP* under low Pi conditions.

Generation of a yeast strain expressing *PHO84* tagged with an HA peptide tag (*RPL18Bpr-PHO84-3XHA*, **Table S4**) was done using the markerless yeast localization and overexpression (MyLO) CRISPR-Cas9 toolkit.[98] This was accomplished by amplification of the *PHO84* coding sequence from BY4742 genomic DNA using primers, PHO84BsaI-F and PHO84BsaI-R, followed by cloning into the BsaI sites of vector pBBK42 by combining 200 ng of BsaI digested *PHO84* DNA with 100 ng of BsaI digested vector and ligating at 16 ˚C for 18 h with T4 DNA ligase. The

resulting construct has the *PHO84* expression driven by the *RPL18B* promoter and is translationally fused to three HA tags on its carboxy-terminal end. The construct was inserted into a safe-harbour site (FF18; chrXV665159..665140) in *pho84*Δ (**Table S4**) by using the vector pBBK18, which encodes Cas9 and a pre-cloned gRNA that targets the cut site to this genomic location. Recombinants were selected on hygromycin and the *PHO84-3XHA* insertion was confirmed by colony PCR using the Phire Plant Direct PCR master mix using primers: BB867-ConLS-F and BB502-SSA1-Chk-R (**Table S5**).

Isolation of RNA and sequencing

For *rac*-GR24-treated samples, a single *S. cerevisiae* colony (EGY48 *MAT*α) was inoculated into liquid YPD media for 17 h. Then, 500 µl of overnight culture was diluted into 5 ml YPD and incubated for a further 2 h. Cells were treated with DMSO (n=3) or 50 µM *rac*-GR24 (n=3) and incubated for a further 2 h until log phase. RNA was extracted following a modified method of (Biss *et al*., 2014).[99] Briefly, cells were washed twice with 5 ml DPEC-treated water and lysed in 350 µl lysis buffer (200 mM Tricine, 500 mM NaCl, 1% SDS, 10mM EDTA) by beating for 1.5 min, resting on ice for 30 s, and repeating this once more. Then, 1 ml TRI Reagent was added and the lysate was centrifuged at 7,000 x *g* at 4˚C for 5 min and the supernatant mixed with 200 µl chloroform. Samples were vortexed for 30 s, incubated at room temperature for 10 min, and centrifuged at 12,000 x g at 4˚C for 15 min. From the resulting upper aqueous phase, 500 µl was mixed with 500 µl 100 % ice-cold isopropanol and incubated at room temperature for 5 min, centrifuged at 12,000 x g for 10 min at 2˚C, and washed twice with 1 ml 75 % ethanol. Finally, RNA was air dried and dissolved in 50 µl DEPC-treated dH_2O. RNA was treated with DNase I at 37˚C for 1 h and subsequently cleaned up using the Monarch® RNA Cleanup kit. Total RNA samples were sent for Illumina sequencing at the Donnell Sequencing Centre (Toronto, CA).

For MeJA treated samples, a single *S. cerevisiae* colony (BY4742 *MAT*α) was inoculated into liquid YPD media and grown overnight until culture reached an OD_{600} ~ 20. A volume of 5 ml cell suspension was pelleted and resuspended in 10 ml fresh YPD. Cells were treated with DMSO (n=3) or 50 µM MeJA (n=3) and incubated for 3 h. Cells were pelleted, resuspended in residual media (~30 µl) and placed on ice. The liquid cell slurry was transferred to a pre-cooled mortar (placed in a liquid nitrogen bath for 2 mins) and ground to a fine powder. Powdered cells were transferred to an Eppendorf tube suspended in liquid nitrogen and stored at -80˚C until

extraction. RNA was extracted using the Qiagen RNeasy Plant Minikit and eluted in 30 µl RNase-free water. RNA was treated with DNase I at 37˚C for 30 mins and subsequently cleaned up using the Qiagen RNeasy MinElute kit. Total RNA samples were sequenced using MGI DNBSEQ platform at the Centre for the Analysis of Genome Evolution and Function (CAGEF, University of Toronto, CA).

RNA sequencing, and differential gene expression analysis

Fastq files were quality checked using FastQC[100] and aligned with HiSat2[101] against the reference transcriptome (file name: GCF_000146045.2_R64_cds_from_genomic.fna) downloaded from the Saccharomyces Genome Database (SGD).[27] Read counts per transcript and Transcript Per Million (TPM) values were generated using Salmon.[102] Read counts were analysed using DESeq2 in R and differentially expressed genes (DEGs) were identified between the treated and mock (DMSO) *S. cerevisiae* samples using the Wald test.[103,104] DEGs were selected as significant if the adjusted p-value < 0.05 and $\log_2$(fold change) > 1 or < -1. DEGs were visualised as a volcano plot, plotted using ggplot2 in R.[103,105] To test for gene annotation category enrichment in the *rac*-GR24 transcriptome, we preformed over-representation analysis on DEGs identified in the transcriptomes. This was performed using SGD Gene Ontology Term Finder, with significance set at FDR ≤ 0.01. *Rac*-GR24-induced DEGs annotated to be involved in phosphate metabolism were compared to a transcriptome in which *S. cerevisiae* was subjected to phosphate starvation conditions for three hours.[106] Methyl jasmonate-induced DEGs annotated to be involved in sugar metabolism were compared to a transcriptome in which *S. cerevisiae* was subjected to varying carbon sources.[107] The $\log_2$ fold change values of the compared treatments were collated into a heatmap using ComplexHeatmap R package.[108]

Profiling *PHO5pr-YFP* reporter expression in *rac*-GR24-treated yeast cells

Yeast carrying the *PHO5pro-YFP* transcriptional fusion was inoculated into 1 ml YNB selective media with 5 mM Pi in a deep 96-well block. After ~ 20 hr growth, OD_{600} was measured and 10 $OD_{600}.ml^{-1}$ units of cell culture was transferred to 1.5 ml Eppendorf tubes. Cells were washed in 1 ml dH_2O and resuspended in 1ml dH_2O. Then, 200 µl cell suspension was diluted in 800 µl 1.25 x fresh YNB selective media supplemented with either 0.5 mM or 5 mM Pi (as described in figure legends), and cultures incubated for 2 h. Then, 20 µl cell culture was diluted

again into wells of a Greiner 96-well clear-bottom black-wall plate containing 80 µl fresh 1.25x YNB selective media with either 0.5 mM or 5 mM Pi, supplemented with either DMSO or *rac*-GR24. Plates were incubated in an Infinite M1000 Pro (TECAN) at 30˚C and subjected to double orbital shaking for 180 s with a 3.5 mm amplitude at 108 rpm. At 10 min intervals, two parameters were recorded for cell suspensions: (i) absorbance at 600 nm (OD_{600}); and (ii) YFP emission intensity at a wavelength of 528 nm following an excitation at 515 nm. Both the excitation and emission bandwidths were set to 5 nm, and the gain to 100. Four measurements were made per well and each treatment was replicated in three wells of the same plate. The YFP emission intensity values were normalised by dividing by the OD_{600} values.

Profiling acid phosphatase activity for yeast grown on solid media

Acid phosphatase activity of yeast grown on solid media was assayed using a staining procedure similar to that described by Toh-E & Oshima (1974).[109] First, a single *S. cerevisiae* colony was inoculated into 1 ml YNB liquid media with 5 mM Pi and incubated for ~ 24 h. A 2 µl drop of saturated culture was spotted onto solid YNB media containing 5 mM Pi supplemented with either DMSO or GR24. For yeast spots shown in Fig. 4F, saturated cell cultures were first washed in 1 ml dH_2O and resuspended in low Pi (0.5 mM) for 4 h prior to spotting. After ~ 20 h growth, spots were stained by overlaying the plate with soft molten agar (0.6 % agar w/v) in 0.05 M acetate buffer (pH 4.0), supplemented with 0.5 $mg.ml^{-1}$ 1-naphthyl phosphate disodium and 0.5 $mg.ml^{-1}$ Fast Blue B. The acetate buffer was made by dissolving 13.6 g sodium acetate and 3 ml glacial acetic acid in 800 ml dH_20, adjusting pH to 4.0 with HCl, bringing final volume to 1 L with dH_20, and then autoclaving. The molten agar solution was cooled to ~ 40˚C prior to gently pouring over the yeast spots. Plates were incubated at room temperature for ~ 30 min prior to imaging, using a dissecting microscope (with a Leica DFC320 camera) or a Nikon D7100 camera.

Microscopy of yeast cells carrying *PHO4-YFP* or *PHO84-EGFP* translational fusions

To visualise Pho4 subcellular localisation, a yeast strain carrying a *PHO4-YFP* translational fusion integrated at the native locus was inoculated into 4 ml YNB media with 5 mM Pi and grown for ~ 18 h. Then, 1 $OD_{600}.ml^{-1}$ of cell suspension was washed twice in dH_2O and resuspended in fresh 0.05 mM Pi YNB -leu (4 % glucose) media to an OD_{600}~1. The cultures were incubated at 30˚C for 4 h and then 1 ml of cell suspension was treated with either DMSO (mock)

or 50 µM *rac*-GR24, plus 5 mM KH_2PO_4 to replenish the Pi in the media. For visualising YFP, 3 µl cell suspension was loaded onto a glass slide and imaged at 63x magnification using a Leica TCS SP5 confocal microscope.

Yeast cells integrated with a *PHO84-EGFP* construct at the native locus were grown in 4 ml YNB media with 5 mM Pi (2 % glucose) media overnight. The following morning, the culture was washed twice in dH_2O and resuspended in fresh 0.05 mM Pi YNB -leu (4 % glucose) media to an OD_{600}~1. Cultures were incubated at 30˚C for 4 h to allow time for *PHO84-EGFP* to accumulate on the plasma membrane. At this point, 1 ml of cell suspension was treated with either DMSO (mock) or 50 µM *rac*-GR24. After the indicated time (see figure legend), 3 µl cell suspension was loaded onto a glass slide for visualising at 63x magnification using a Leica TCS SP5 confocal microscope.

Assaying manganese sensitivity in yeast

Wildtype and *pho84*Δ yeast strains were grown in the same way as described for the AP experiment in Figure 4F. Prior to spotting, cells were washed in dH_2O, adjusted to an OD_{600} of 10, and spotted as a 5-fold serial dilution onto YPD media supplemented with 8 mM $MnCl_2$ with or without 50 µM *rac*-GR24. Plates were incubated at 30˚C and imaged at 48 h with a Nikon D7100 camera.

***Rac*-GR24 yeast killing assay**

Single yeast colonies were inoculated into 3 ml YNB –trp –leu supplemented with 5 mM Pi. After 24 h growth at 30˚C, 2 µl of saturated culture was inoculated onto YNB –trp –leu solid media supplemented with 5 mM Pi, the carbon source indicated in the respective figure, and either DMSO or *rac*-GR24. For strains grown on glucose as a sole carbon source, images of yeast growth were taken ~ 20 h after spotting. For strains grown on galactose as a sole carbon source, images were taken ~ 44 h after spotting. Images were taken with a dissecting microscope fitted with a Leica DFC320 camera.

***PHO84* PCR mutagenesis and *rac*-GR24 insensitivity screen**

A *PHO84* mutant library was constructed using the method established by Weir.[110] Briefly, primers were designed to amplify the *PHO84pr-PHO84* fragment from pAG413m-*PHO84pr-*

PHO84. These primers bind approximately 500 bp upstream and downstream of the insert and attach long arms of homology to the pAG vector series. With these primers, error-prone PCR was performed with the standard Taq (FroggaBio Taq DNA Polymerase) recipe with altered dNTP concentrations: dATP (0.2 μM), dGTP (0.2 μM), dCTP (1 mM), and dTTP (1 mM). Additionally, the reaction was supplemented with 5 mM $MgCl_2$.

The EY917 strain was transformed with the PCR-mutagenized *PHO84pr-PHO84* amplicons and the pAG415m plasmid backbone digested with HindIII and XhoI. Strains carrying a functional copy of Pho84 and a correctly assembled plasmid were identified by plating the transformed yeast onto YNB –trp –leu. After two days of growth at 30˚C, colonies were picked and individually inoculated into YNB –trp –leu media in deep 96-well plates. Using a 96-point pin tool, the cultures were stamped onto OmniTrays^{TM} containing YNB –leu –trp supplemented with 100 μM *rac*-GR24. Spots containing resistant mutants were identified after ~ 24 h growth and retested. Genomic DNA was extracted from successful retests and the *PHO84pr-PHO84* insert was amplified using primers specific to the pAG415m-*PHO84pr-PHO84* plasmid. The insert was sequenced at the Centre of Applied Genomics (Toronto, Canada).

Identification of causative SL insensitive mutations and site-directed mutagenesis

To identify mutations causing SL insensitivity, the *PHO84* ORF was split into three ~ 600 bp sectors. These sectors were chosen such that only a single mutation would fall within their borders. Primers were designed so that each sector could be individually amplified and then recombined with wild type copies of the other two (**Table S5**; **Figure S8**). For instance, to determine if a mutation in sector 1 was causative, two PCRs would be performed: (1) the first (red primers) uses mutant plasmid as a template and (2) the second (yellow forward primer and blue reverse primer) uses a wildtype plasmid as a template (**Figure S8**). These two PCR products would then be used for gap-repair cloning (described below) into a linearized pAG415m plasmid (**Figure S8**). To avoid any inappropriate recombination with the wildtype *PHO84* allele, all gap-repair cloning was carried out in the BY4742 *pho84Δ* strain (**Table S4**). Plasmids were isolated from the yeast as described above in the gap-repair cloning section. Correct assembly was verified by sequencing the insert. Each construct was then moved into the EY917 genotype and the GR24 killing assay performed (described above).

For site-directed mutagenesis of *PHO84*, forward (pAG413-Up-Homology) and reverse (pAG413-Down-Homology) primers (**Table S5**) were designed so that they both contained the desired mutation and collectively spanned at least 30 bp (**Figure S8**). These primers were then paired with reverse and forward primers which bind 500 bp upstream and downstream of the insert and attach long arms of homology to the pAG vector series (**Table S5**). These two primer pairs (orange and purple in **Figure S8**) were then used for PCR. The PCR products were then used for gap-repair cloning with a linearized pAG415m plasmid (**Figure S8**). Correct assembly was verified by sequencing the insert. Each construct was then moved into the EY917 genotype and the GR24 killing assay performed (described above).

Yeast gap-repair cloning

To perform gap-repair cloning, primers were designed for each insert such that each end of the amplicon has at least 30 bp of homology to the destination vector.[96] For multiple inserts, primers were designed so that the outer two PCR products had at least 30 bp of homology to the destination vector as well as homology to the other insert. For each insert, a 20 µl PCR was prepared. Additionally, the destination vector was digested with two different restriction enzymes, which were heat inactivated after the reaction. The uncleaned PCR and digest products are then directly transformed into yeast according to the lithium acetate approach described above. To isolate plasmids, 1 ml of saturated overnight yeast culture was spun down and resuspended in 120 µl of sorbitol-EDTA buffer (0.9 M sorbitol, 0.1 M EDTA, pH = 8) containing 10 units of zymolyase or lyticase. The suspension was then incubated at 37°C for 1 h. After digestion, the spheroplasts were spun at 3,000 rpm for 5 min in a microcentrifuge. The supernatant was decanted, and the plasmid was removed from the spheroplasts using the NEB Monarch® Plasmid Miniprep Kit. Purified plasmids were then transformed into *E. coli* for storage and propagation.

Pi uptake assays

For P^{32} uptake assays, yeast strains were grown overnight in YPD media to saturation. The cultures were split in half, either DMSO or *rac*-GR24 was added, and cells were further incubated for 4 h. Cells were pelleted and resuspended in fresh YNB with 5 mM Pi to an OD_{600} ~ 4 with DMSO or *rac*-GR24. For each sample, 100 µl cell suspension was added to an Eppendorf tube with 900 µl fresh YNB media containing radiolabelled P^{32} as a tracer. To determine the specific

radioactivity at point of experiment, we also obtained total Counts Per Minute (CMP) for media without cells but containing the same volume of radiolabelled tracer. Cells were incubated at 30˚C for 10 min, transferred to ice for 1 min, and then pelleted. The supernatant was removed by aspiration and 1 ml ice-cold dH_2O was added. Cells were vortexed for 1 min, pelleted and resuspended in a final volume of 100 µl ice-cold dH_2O. The cell suspension was transferred to a scintillation vial with 5 ml scintillation fluid and CPM obtained using a TRICARB 3170 TR/SL (Perkin Elmer). CPM were expressed as picomole of P^{32} per minute per OD_{600} unit.

For Pi supernatant depletion measurements, yeast was grown in YPD media overnight. Ten $OD_{600}.ml^{-1}$ were resuspended in 1 ml of fresh YPD media, treated with DMSO or 50 µM *rac*-GR24 and further incubated for 4 h. Then, 10 $OD_{600}.ml^{-1}$ of cells were pelleted and the supernatant was collected to measure Pi in the media according to the molybdenum blue method.[111] Briefly, 25 µl of the supernatant from treated and non-treated yeast cultures (plus fresh media as the initial reference for Pi concentration) was added to glass tubes containing 1 ml of solution A (0.1 M ascorbic acid; 0.5 M trichloroacetic acid). Then, 200 µl of solution B (0.01 M ammonium molybdate) followed by 500 µl of solution C (0.1 M sodium citrate; 0.2 M sodium arsenite; 5 % acetic acid) was added and solutions were mixed by pipetting. Samples (200 µl volume) were loaded into a 96-well plate and the absorbance at 700 nm was measured in a plate reader (xMark Microplate Spectrophotometer, BioRad). The change in Pi in the media was obtained by subtracting the value of Pi in the media of treated and non-treated cells from the value obtained for fresh media and then normalized by dividing the OD_{600}. The cell pellet that was obtained from this experiment was reserved for polyP extraction (see below).

Binding assay using whole cells

Strains expressing either *PHO89* (EY917 *p5819-PHO89*) or *PHO84* (EY917 *p5587-PHO84*) (**Table S4**) were grown for 18 h at 30˚C in Yeast Nitrogen Base (YNB) without amino acids and without phosphate (0.59 % (w/v), supplemented with an amino acid mix lacking leucine and tryptophan, 2 % (w/v) glucose, and 0.5 mM sodium phosphate. Cells were harvested by centrifugation at 4000 x *g* for 5 min and resuspended in the same medium at an OD_{600} = 1. For each strain, aliquots of 0.75 ml were dispensed into three separate Eppendorf tubes on ice. Then, 1 µM [H_3]-GR24 was added, the tubes were mixed by inversion and incubated on ice for 30 min. The inversions were repeated every 10 min of incubation. Following incubation, the tubes were

centrifuged at 16,000 x *g* in a pre-cooled centrifuge and transferred to an ice bath. The supernatant from each was carefully removed without touching the cell pellets. The tubes were then transferred to a rack and 0.24 ml of 100 % ethanol was added to each tube. The tubes were vortexed at room temperature (24˚C) for 1 h. Following this step, the tubes were centrifuged for 1 min at 16 000 x *g*. Exactly 0.2 ml of each supernatant was transferred to scintillation vials to which 5 ml of UltimaGold scintillation cocktail was added. Samples were counted for 5 min each with a Hidex 300 SL automatic liquid scintillation counter.

Drug affinity responsive target stability (DARTs) assay

For drug affinity responsive target stability (DARTS) assays, Pho84-3xHA protein was prepared in the following way. The yeast strain *RPL18Bpr-PHO84-3xHA* (**Table S4**) was grown for 18 h at 30˚C in 200 ml low phosphate YPD medium, which was made by dissolving 5 g yeast extract, 10 g peptone, 1.23 g $MgSO_4$ in 475 ml ddH_2O, followed by slowly adding 4 ml concentrated NH_4OH to precipitate the salts. The solution is then vacuum filtered through a 0.22 mm nitrocellulose filter, adjusted to pH 6.5 with HCl and autoclaved prior to addition of filter sterile glucose to a final concentration of 2 %. Cells were harvested by centrifugation (3000 x *g;* 3 min) and the cell pellet was washed by resuspension in 50 ml ddH_2O followed by centrifugation. Cells were then resuspended in 35 ml ice cold lysis buffer which consisted of 50 mM HEPES-KOH (pH 7.5), 100 mM NaCl, 5 mM $MgCl_2$, 5 mM dithiothreitol, 10 % glycerol. The cells were lysed by two passages in a French pressure cell (Thermo Electron Corporation; FA-032) at 2000 PSIs. The lysate was centrifuged at 4˚C at 5,000 x *g* for 10 min to remove any unbroken cells and/or cell wall fragments. The supernatant was then centrifuged at 100,000 x *g* at 4˚C for 1 h to collect cell membranes. Following this step, the supernatant was discarded, and the membrane pellet was resuspended in lysis buffer using a glass homogenizer at a concentration of 10 µg/µl of protein. Protein concentration was determined using a Bradford assay. (Kielkopf CL, Bauer W, Urbatsch IL. Bradford Assay for Determining Protein Concentration.[112]

DARTS assays were carried out by combining 230 µg membrane proteins, 1 µl of *rac*-GR24 to 50 µM or 1 µl DMSO to a final volume of 25 µl, and incubating the mixture at 30˚C for 30 min. This incubation was followed by addition of 1 µl of pronase, which was diluted in water at different concentrations (1/10, 1/20, 1/30, 1/40, 1/50) from a 10 $mg.ml^{-1}$ stock. A negative control was included where 1 µl of water was added instead of a pronase dilution. Each of the

samples were incubated at 22˚C for 30 min. The reactions were stopped by adding an equal amount of 2x SDS-urea sample buffer which consisted of 80 mM Tris-Cl, pH 6.8, 2 % SDS, 8 M urea, 10 % glycerol, 0.1 M DTT, 0.00006 % bromophenol blue) and followed by incubating the samples at 37˚C for 30 min. To assess protein stability, 20 µl of each sample was loaded onto 12 % polyacrylamide SDS gels which were either stained with Coomassie Brilliant Blue R or blotted onto Polyvinylidene fluoride (PVDF) membranes for western blot analysis. For western blots, proteins were transferred using a semi-dry transfer system (BioRad; 1704150) for 30 min at 25 V with a buffer consisting of 24 mM Tris, 192 mM glycine, 20 % methanol. Blots were blocked by incubating them at 22˚C for 1 h with 3 % (w/v) skim milk in TBST (10 mM Tris-Cl, pH 7.4, 0.9 % (w/v) NaCl, 0.02 % (v/v) Tween 20. This was followed by incubation for 16 h at 4˚C with Anti-HA horse radish peroxidase (HRP) conjugated antibody diluted 2000x in the same buffer. The blots were then washed three times for 10 min at 22˚C with TBST before developing and visualizing antibody dependent signal with a luminol-based chemiluminescent substrate (Thermo Fisher; 34075).

PolyP extraction

Cell pellets from 10 $OD_{600}.ml^{-1}$ of cells were resuspended in 400 µl of ice-cold AE buffer (50 mM sodium acetate (pH 5.3); 10 mM EDTA). Cells were lysed by adding 300 µl of phenol (saturated pH 6.6/7.9 Biotech Grade) and 20 µl of 20 % SDS. Cells were homogenized and incubated at 65°C for 5 min followed by 1 min on ice. Then, 300 µl of chloroform was added, homogenized by inverting and centrifuged for 2 min at max speed (room temperature). From the upper phase, 450 µl was transferred to a fresh tube, and 350 µl of chloroform was added. Samples were homogenized by inverting and centrifuged again for 2 min at max speed (room temperature). From the upper phase, 400 µl was recovered and treated with 1 µl of RNase A (10 $mg.ml^{-1}$) and 1 µl of DNase I (10 $mg.ml^{-1}$) for 1 h at 37°C. After incubation, 1 ml of absolute ethanol and 40 µl of 3 M sodium acetate (pH 5.3) was added and incubated at -20°C for 3 h to precipitate the polyP. Then, samples were centrifuged for 20 min at max speed (4°C), the supernatant was discarded, and the pellet washed with 500 µl of 70 % ethanol. Samples were centrifuged again for 10 min at max speed (4°C). The supernatant was removed, the pellet was air dried and resuspended in 40 µl of Milli-Q water.

PolyP samples were analysed using SDS-PAGE. An SDS-PAGE gel (20 % polyacrylamide gel (acrylamide 10:1 bis-acrylamide) containing 7 M urea in TBE buffer) was loaded with 10 µl of sample mixed with 10 µl of sample buffer (2x TBE; 20 % glycerol; 0.006 % (w/v) bromophenol blue). The gel was run for 2 h at fixed 150 volts (initial current around 11 mA) using TBE buffer. The gel was incubated in staining solution (50 mM TrisHCl pH 10.5; 25 % methanol; 5 % glycerol; 0.01 % Toluidine Blue) for approximately 30 min and distained (50 mM TrisHCl pH 10.5; 25 % methanol; 5 % glycerol) until bands were visible. Images were taken on Chemidoc Image System (BioRad).

Metabolite extraction from GR24-treated yeast

Yeast were cultivated in liquid SD media (5 $g.l^{-1}$ ammonium sulfate, 1.7 $g.l^{1}$ Yeast Nitrogen base, 20 $g.l^{-1}$) with 2 % glucose at 30˚C with shaking at 250 rpm. Both the BY4741 *pho84*Δ and wildtype yeast (**Table S4**) were transformed with the pHLUM minichromosome[113] to restore prototrophy with transformations performed as described previously.[114] BY4741 wildtype and *pho84*Δ strains were grown to a target OD_{600} of 1 with more than two cell doublings between inoculation and harvesting. Cultivation was performed in 15 ml culture tubes with a total culture volume of 5 ml. At the point of sampling, 1 $OD_{600}.ml^{-1}$ of each culture was sampled by vacuum separation of the yeast from the media using PVDF filter membranes. The resulting cell pellets were extracted for 1 h at -20 °C in 2 ml of extraction solution (40 % (v/v) HPLC-grade acetonitrile, 40 % (v/v) HPLC grade methanol 20 % (v/v) HPLC-grade water. The cells were then treated with either a vehicle control (0.1 % DMSO (v/v)) or with 25 µl of *rac*-GR24. Cells were sampled as described above after a treatment duration of 30 and 60 min. Completed extractions were separated from cellular debris by 1 min of centrifugation with a force of 2,254 rcf before being stored at -80 °C until measurement.

Metabolomic profiling

Flow injection analysis time-of-flight mass spectrometry was performed using an Agilent 6550 Series quadrupole time-of-flight mass spectrometer (Agilent) by and adaptation of the method described by Fuhrer *et al*.[115] Analysis was performed using an Agilent 1100 Series HPLC system (Agilent) coupled to a Gerstel MPS 3 autosampler (Gerstel). The mobile phase flow rate was set of 0.15 $ml.min^{-1}$, with the isocratic phase composed of 60:40 (v/v) isopropanol and water

buffered to a pH of 9 with 4 mM ammonium fluoride. Online mass axis correction was performed with taurocholic acid and Hexakis (1H, 1H, 3H-tetrafluoropropoxy)–phosphazne)) within the mobile phase. The instrument was run in 4 GHz mode for maximum resolution while collecting mass spectra between 50 and 1000 m/z. Mass spectrum centroiding, merging, and ion annotation was performed as described in Fuhrer *et al.*[115] with annotations performed against the KEGG *S. cerevisiae* metabolite database.[116] Raw ion intensities were normalized to counteract temporal drifts. The normalized ion intensities were subjected to differential analysis where $\log_2$-transformed fold-changes in ion intensities were calculated for each duration of *rac*-GR24 treatment compared to the untreated control.

Construction of phylogenetic tree of Pho84 homologs

Pho84 homologs from the fungal kingdom were retrieved via BLAST+ [117] in the Uniprot[118] and FungiDB[119] databases. BLAST hits with an e-value threshold 10^{-32} were used in a reciprocal BLAST against a reference *S. cerevisiae* proteome with the same e-value threshold. Alignment of 1,165 Pho84 homologs was done using MUSCLE.[120] Phylogenetic tree construction was performed using RaXML 8.2.[121] The tree was constructed unrooted, using the PROTGAMMAAUTO parameter to select the appropriate model, and otherwise default parameters. Twenty Maximum Likelihood (ML) searches were performed and bootstrapped 100 times. Visualization of the tree and the sequence heatmap was created using the ggtree R package.[122] Sequence logo was created using the ggseqlogo R package.[123]

Modelling of yeast Pho84 and World Health Organisation fungal priority pathogen Pho84 homologs

Modelling of yeast Pho84 was performed using SWISS-MODEL.[124] The occluded form was done with a template model of the Pho84 homolog from *S. indica* (PDB code: 7SP5). The outward-open form was modelled using a template model of *E. coli* glycerol-3-phosphate transporter (PDB code: 1PW4). The inward-open form was modelled using a template model of *E. coli* fucose symporter (PDB code: 3O7Q). Visualizations of protein models were created using PyMol.[125]

Modelling yeast low-affinity phosphate transporters

Modelling of low-affinity phosphate transporters from yeast was retrieved from the AlphaFold Database.[126,127] Highest confidence models were chosen for each protein. Alignment of low-affinity phosphate transporters and Pho84 was performed using MUSCLE.[120] Visualizations of protein models were created using PyMol.[125]

Molecular docking analysis

Docking of SL variants into Pho84 was done using Autodock Vina 4.2.[128] A bounding box was created around the suspected binding pocket region for targeted docking. The best docking pose was chosen in each simulation. PyMol was used to ensure no clashes occurred in the docking poses. Participating amino acids in the docking pose were analyzed using LigPlot+ 2.2.[129]

Screening of fungi library

Soil-dwelling fungi were isolated from soils sampled from various regions in Japan, and the fungal library consisting of 315 strains was used for SL response screening. The fungal strains were grown on potato dextrose agar (PDA) plates, and cylindrical blocks (Φ7 mm) collected from the plate cultures were stored at -80˚C. The library of 315 fugal strains were first grown on PDA media for around 10 d at room temperature. Two blocks containing mycelia were collected from the edge of colonies with sterile straws and inoculated on PDA media containing 1 µM (+)-GR24 or DMSO in 9 cm Petri dishes. Images were taken after 15 d of incubation and strains with visible phenotype on GR24 plates were marked as positives.

Phylogenetic analysis of fungal species

Genomic DNA was extracted by hot-alkaline DNA extraction method as described previously[130]. In brief, mycelia taken from growing colony were suspended in 100 µl of 50 mM NaOH and incubated for 15 min at 95°C. After neutralization with 11 µl of 1 M Tris-HCl (pH 7.5) and dilution by adding 900 µl of distilled water, 0.25 µl was taken as a template for PCR amplification of nuclear ribosomal internal transcribed spacer (ITS) region with primers ITS-5 and ITS-4 (**Table S5**).[131] PCR products were purified with Wizard SV Gel and PCR Clean-up System (Promega) and used as a template for sanger sequencing with SupreDye Cycle Sequencing Kit. The DNA sequencing was performed at sequencing facility in the Center for Gene Research at Nagoya University. The species were identified by BLAST-searching of the ITS region. In the

case that the ITS region was insufficient for taxonomic classification, D1/D2 regions were amplified by PCR with primers NL-1 and NL-4 (**Table S5**) and sequenced for BLAST search. The combination of ITS and D1/D2 led the classification of all the 71 GR24-responsive strains along with 95 randomly chosen strains from the rest of the library.

***Serendipita indica* experiments**

S. indica was prepared for experimentation by first inoculating an 8 mm-diameter plug of fungus onto a PDA plate for ~ 6 d at 30˚C, at which point the fungus had grown to the circumference of the plate. PDA plates were made by dissolving 24 g Potato Dextrose Broth in 1 L dH_2O and autoclaving. Agar was added to a final concentration of 1.5 % (w/v). To assay manganese sensitivity, 8 mm-diameter fungal plugs were excised from the circumference of a plate with a cork-borer and placed upside-down on 8 ml solid PDA media (pH 5.4) supplemented with 0.75 mM $MnCl_2$ with DMSO or 5 µM *rac*-GR24. Plates were incubated at 30˚C for 6 d and imaged with a Nikon D7100 camera.

To assay AP activity, four fungal plugs were homogenised at full speed for 30 s in 2 ml dH_2O in a 15 ml Falcon tube, and then 20 µl fungal homogenate was dispensed onto 1 ml synthetic media containing 1 mM Pi in a 24 well plate. The synthetic media was made according to Sugiura *et al*. (2021)[132], except all Pi sources were omitted and KH_2PO_4 was added as the sole Pi source. Plates were incubated at 30˚C for 48 h and then stained for AP activity as described for yeast.

***Fusarium graminearum* experiments**

For *Fusarium* experiments, a minimal medium was prepared as follows (per litre of dH_2O): 0.5 g $MgSO_4 \cdot 7H_2O$; 0.5 g KCl; 20 g agar; 30 g sucrose; 2 g KNO_3; 1 mL 0.5 M MES (pH 5); and 0.2 ml trace element solution.[133] The trace element solution was prepared as follows (per litre of dH_2O): 5 g citric acid; 5 g $ZnSO_4 \cdot 6H_2O$; 1 g $Fe(NH_4)_2(SO_4)_2 \cdot 6H_2O$; 250 mg $CuSO_4 \cdot 5H_2O$; 50 mg $MnSO_4$; 50 mg H_3BO_3; 50 mg $Na_2MoO_4 \cdot 2H_2O$.[133] After autoclaving, the media was poured into the 9 ml plates.

For the Pi dose response, KH_2PO_4 (pH = 5) was added to these plates to reach final concentrations of 10 mM, 1 mM, 0.1 mM, 0.01 mM, and 0 mM respectively. Additionally, for each KH_2PO_4 concentration, 9 ml of DMSO or 5 µM GR24 was added. After the agar solidified 1 ml of *F. graminearum* spores were spotted onto the centre of plates, which were then incubated

for 5–6 d at room temperature in a dark cabinet. *Fusarium* plates were photographed with a Nikon D7100 camera.

For manganese assays, minimal media was prepared as described above, except the final KH_2PO_4 concentration was adjusted to 5 mM and the pH to 6.4. To each plate, 10 ml of minimal media was added along with 100 ml of freshly prepared 1 M $MnCl_2$ and either 10 µl DMSO or 10 µl 5 mM *rac*-GR24. After the agar solidified 1 ml of *F. graminearum* spores were spotted onto the centre of plates, which were then incubated for 5–6 d at room temperature in a dark cabinet. *Fusarium* plates were photographed with a Nikon D7100 camera.

For the *Fusarium* spore experiments, *F. graminearum* NRRL29169 is the wildtype strain and is the parental strain for the construction of *FgPHO84* knockout (Δ*FGSG_07894*). To construct Δ*FGSG_07894* by CRISPR/Cas9, two crRNAs (crRNAup: GATCTCAGACTGTGTCTCTGTGG and crRNAdn: GTGGTACATCAGAATGCCTTGGG) were designed for *FGSG_07894* using EuPaGDT[134] with DOAM 233423 as reference genome. The repair template was generated by PCR of the resistance marker hygromycin by the microhomology primers: MH-F and MH-R (**Table S5**). MH primers were designed with 50 bp specificity to the upstream and downstream PAM sites defined by each crRNA respectively and share 19–21 bp homology to the hygromycin sequence, which was amplified by PCR. The ribonucleoprotein complex (Cas9-gRNA complex) was assembled *in vitro* by mixing each crRNA, the tracrRNA, and the Cas9 nuclease. After incubation, the complex was incubated with *F. graminearum* protoplasts to generate transformants. To confirm the *ΔFGSG_07894* mutant strain, genomic DNA from wildtype and mutant strains were PCR amplified with gene specific primers: Int-F and Int-R (**Table S5**). In addition, the marker gene (hygromycin) was amplified in the mutant strain with primers: Hyg-F and Hyg-R (**Table S5**). Macroconidia were produced in SNA medium (per litre): 1 g KH_2PO_4, 1 g KNO_3, 0.5 g $MgSO_4 \cdot 7H_20$, 0.5 g KCl, 0.2 g glucose, 0.2 g sucrose, 1.5 % agar. For experiments involving *rac*-GR24, the spores were cultured in 25 ml SNA medium lacking KH_2PO_4. Spores were harvested and counted after 7 d incubation. Conidiophores (1000 spores/ml) were germinated in 4 ml potato dextrose broth in a 6-well culture plate at 28°C, shaking at 160 rpm in the dark. Germination was monitored over time and photographed 40x by EVOS XL Core imaging system (Thermo Fisher, Canada).

Quantification and Statistical Analysis

Quantification of acid phosphatase data was done using ImageJ.[135] T-tests were performed using stats package in R.[103]

Fig. 4D – Pi uptake by P32:

Significance of difference between DMSO and *rac*-GR24 was measured using a two-sample t-test ($t = 40.46$; $df = 13.80$; $p < 0.001$).

Fig. 4E – Pi uptake by molybdate blue:

Significance of difference between DMSO and *rac*-GR24 was measured using a two-sample t-test ($t = 11.70$; $df = 21.29$; $p < 0.001$).

Fig. 4G – PHO5pr-YFP assay:

Significance of difference between DMSO and (+)-(2'R)-GR24 was measured using a two-sample t-test (2.5 µM: $t = 4.38$; $df = 9.15$; $p < 0.005$, 5 µM: $t = 19.91$; $df = 10.65$; $p < 0.0001$, 10 µM: $t = 24.31$; $df = 4.44$; $p < 0.0001$, 15 µM: $t = 23.37$; $df = 3.69$; $p < 0.0001$).

Fig. 5F – H^3-*rac*-GR24 binding assay:

Significance of difference between *EY917-PHO89* and *EY917-PHO84* was measured using a two-sample t-test ($t = -12.333$; $df = 2.1886$; p-value < 0.005)

Fig. 7B – Serendipita colony area:

Significance of difference between DMSO and *rac*-GR24 was measured using a two-sample t-test ($t = -10.943$; $df = 13.8$; p-value < 0.001).

Fig. 7E – Fusarium spore count:

Significance of difference between DMSO and *rac*-GR24 was measured using a two-sample t-test (wild-type: $t = -17.331$; $df = 3.5918$; p-value <= 0.001, *Fgpho84*Δ: $t = -2.2997$; $df = 6.2281$; p-value >= 0.05). Significance of difference between untreated wild type and *Fgpho84*Δ was measured using a two-sample t-test ($t = -3.7326$; $df = 6.8342$; p-value <= 0.01).

Supplemental Tables

Table S1. List of naturally occurring fungi tested for response to Strigolactone: Related to Figure 2, Figure S2.

Table S2. Differentially expressed genes in response to (+)-(2'R)-GR24 and Methyl Jasmonate: Related to Figure 3A, Figure S6.

Table S3. Processed flow injection mass spectrometry data: Related to Figure 4B.

Table S4. List of yeast strains used in this study: Related to STAR methods.

Table S5. List of primers used in this study: Related to STAR methods.

References

1. Mukherjee, S., and Bassler, B.L. (2019). Bacterial quorum sensing in complex and dynamically changing environments. Nat Rev Microbiol *17*, 371–382. https://doi.org/10.1038/s41579-019-0186-5.
2. Fleischer, J., and Krieger, J. (2018). Insect Pheromone Receptors – Key Elements in Sensing Intraspecific Chemical Signals. Front. Cell. Neurosci. *12*, 425. https://doi.org/10.3389/fncel.2018.00425.
3. Tumlinson, J.H. (2023). Complex and Beautiful: Unraveling the Intricate Communication Systems Among Plants and Insects. Annu. Rev. Entomol. *68*, 1–12. https://doi.org/10.1146/annurev-ento-021622-111028.
4. Venturi, V., and Keel, C. (2016). Signaling in the Rhizosphere. Trends in Plant Science *21*, 187–198. https://doi.org/10.1016/j.tplants.2016.01.005.
5. Leach, J.E., Triplett, L.R., Argueso, C.T., and Trivedi, P. (2017). Communication in the Phytobiome. Cell *169*, 587–596. https://doi.org/10.1016/j.cell.2017.04.025.
6. O'Banion, B.S., O'Neal, L., Alexandre, G., and Lebeis, S.L. (2020). Bridging the Gap Between Single-Strain and Community-Level Plant-Microbe Chemical Interactions. MPMI *33*, 124–134. https://doi.org/10.1094/MPMI-04-19-0115-CR.
7. Eichmann, R., Richards, L., and Schäfer, P. (2021). Hormones as go-betweens in plant microbiome assembly. The Plant Journal *105*, 518–541. https://doi.org/10.1111/tpj.15135.
8. Lu, Y., Wang, E., Tang, Z., Rui, J., Li, Y., Tang, Z., Dong, W., Liu, X., George, T.S., Song, A., et al. (2022). Roots and microbiome jointly drive the distributions of 17 phytohormones in the plant soil continuum in a phytohormone-specific manner. Plant Soil *470*, 153–165. https://doi.org/10.1007/s11104-021-04898-w.
9. Costacurta, A., and Vanderleyden, J. (1995). Synthesis of Phytohormones by Plant-Associated Bacteria. Critical Reviews in Microbiology *21*, 1–18. https://doi.org/10.3109/10408419509113531.
10. Spaepen, S. (2015). Plant Hormones Produced by Microbes. In Principles of Plant-Microbe Interactions, B. Lugtenberg, ed. (Springer International Publishing), pp. 247–256. https://doi.org/10.1007/978-3-319-08575-3_26.

11. Tudzynski, B., and Sharon, A. (2002). Biosynthesis, Biological Role and Application of Fungal Phytohormones. In Industrial Applications, H. D. Osiewacz, ed. (Springer Berlin Heidelberg), pp. 183–211. https://doi.org/10.1007/978-3-662-10378-4_9.
12. Chanclud, E., and Morel, J. (2016). Plant hormones: a fungal point of view. Molecular Plant Pathology *17*, 1289–1297. https://doi.org/10.1111/mpp.12393.
13. Spence, C., and Bais, H. (2015). Role of plant growth regulators as chemical signals in plant–microbe interactions: a double edged sword. Current Opinion in Plant Biology *27*, 52–58. https://doi.org/10.1016/j.pbi.2015.05.028.
14. Kazan, K., and Lyons, R. (2014). Intervention of Phytohormone Pathways by Pathogen Effectors. Plant Cell *26*, 2285–2309. https://doi.org/10.1105/tpc.114.125419.
15. Nagahama, K., Ogawa, T., Fujii, T., and Fukuda, H. (1992). Classification of ethylene-producing bacteria in terms of biosynthetic pathways to ethylene. Journal of Fermentation and Bioengineering *73*, 1–5. https://doi.org/10.1016/0922-338X(92)90221-F.
16. Han, X., and Kahmann, R. (2019). Manipulation of Phytohormone Pathways by Effectors of Filamentous Plant Pathogens. Front. Plant Sci. *10*, 822. https://doi.org/10.3389/fpls.2019.00822.
17. Boiero, L., Perrig, D., Masciarelli, O., Penna, C., Cassán, F., and Luna, V. (2007). Phytohormone production by three strains of Bradyrhizobium japonicum and possible physiological and technological implications. Appl Microbiol Biotechnol *74*, 874–880. https://doi.org/10.1007/s00253-006-0731-9.
18. Jacobs, S., Zechmann, B., Molitor, A., Trujillo, M., Petutschnig, E., Lipka, V., Kogel, K.-H., and Schäfer, P. (2011). Broad-Spectrum Suppression of Innate Immunity Is Required for Colonization of Arabidopsis Roots by the Fungus *Piriformospora indica*. Plant Physiology *156*, 726–740. https://doi.org/10.1104/pp.111.176446.
19. Pieterse, C.M.J., Van Der Does, D., Zamioudis, C., Leon-Reyes, A., and Van Wees, S.C.M. (2012). Hormonal Modulation of Plant Immunity. Annu. Rev. Cell Dev. Biol. *28*, 489–521. https://doi.org/10.1146/annurev-cellbio-092910-154055.
20. Xu, G., Yang, S., Meng, L., and Wang, B.-G. (2018). The plant hormone abscisic acid regulates the growth and metabolism of endophytic fungus Aspergillus nidulans. Sci Rep *8*, 6504. https://doi.org/10.1038/s41598-018-24770-9.

21. Prusty, R., Grisafi, P., and Fink, G.R. (2004). The plant hormone indoleacetic acid induces invasive growth in *Saccharomyces cerevisiae*. Proc. Natl. Acad. Sci. U.S.A. *101*, 4153–4157. https://doi.org/10.1073/pnas.0400659101.

22. Dor, E., Joel, D.M., Kapulnik, Y., Koltai, H., and Hershenhorn, J. (2011). The synthetic strigolactone GR24 influences the growth pattern of phytopathogenic fungi. Planta *234*, 419–427. https://doi.org/10.1007/s00425-011-1452-6.

23. Akiyama, K., Matsuzaki, K., and Hayashi, H. (2005). Plant sesquiterpenes induce hyphal branching in arbuscular mycorrhizal fungi. Nature *435*, 824–827. https://doi.org/10.1038/nature03608.

24. Smith, J.E. (2009). Mycorrhizal Symbiosis (Third Edition). Soil Science Soc of Amer J *73*, 694–694. https://doi.org/10.2136/sssaj2008.0015br.

25. Helfer, S. (2014). Rust fungi and global change. New Phytologist *201*, 770–780. https://doi.org/10.1111/nph.12570.

26. Lee Taylor, D., and Sinsabaugh, R.L. (2015). The Soil Fungi. In Soil Microbiology, Ecology and Biochemistry (Elsevier), pp. 77–109. https://doi.org/10.1016/B978-0-12-415955-6.00004-9.

27. Cherry, J.M., Hong, E.L., Amundsen, C., Balakrishnan, R., Binkley, G., Chan, E.T., Christie, K.R., Costanzo, M.C., Dwight, S.S., Engel, S.R., et al. (2012). Saccharomyces Genome Database: the genomics resource of budding yeast. Nucleic Acids Research *40*, D700–D705. https://doi.org/10.1093/nar/gkr1029.

28. Botstein, D., and Fink, G.R. (2011). Yeast: An Experimental Organism for 21st Century Biology. Genetics *189*, 695–704. https://doi.org/10.1534/genetics.111.130765.

29. Parsons, A.B., Lopez, A., Givoni, I.E., Williams, D.E., Gray, C.A., Porter, J., Chua, G., Sopko, R., Brost, R.L., Ho, C.-H., et al. (2006). Exploring the Mode-of-Action of Bioactive Compounds by Chemical-Genetic Profiling in Yeast. Cell *126*, 611–625. https://doi.org/10.1016/j.cell.2006.06.040.

30. Butcher, R.A., and Schreiber, S.L. (2006). A microarray-based protocol for monitoring the growth of yeast overexpression strains. Nat Protoc *1*, 569–576. https://doi.org/10.1038/nprot.2006.80.

31. Ericson, E., Hoon, S., St.Onge, R.P., Giaever, G., and Nislow, C. (2010). Exploring Gene Function and Drug Action Using Chemogenomic Dosage Assays. In Methods in Enzymology (Elsevier), pp. 233–255. https://doi.org/10.1016/S0076-6879(10)70010-0.
32. Liti, G. (2015). The fascinating and secret wild life of the budding yeast S. cerevisiae. eLife *4*, e05835. https://doi.org/10.7554/eLife.05835.
33. Jouhten, P., Ponomarova, O., Gonzalez, R., and Patil, K.R. (2016). *Saccharomyces cerevisiae* metabolism in ecological context. FEMS Yeast Research *16*, fow080. https://doi.org/10.1093/femsyr/fow080.
34. Warringer, J., Zörgö, E., Cubillos, F.A., Zia, A., Gjuvsland, A., Simpson, J.T., Forsmark, A., Durbin, R., Omholt, S.W., Louis, E.J., et al. (2011). Trait Variation in Yeast Is Defined by Population History. PLoS Genet *7*, e1002111. https://doi.org/10.1371/journal.pgen.1002111.
35. Li, H., and Johnson, A.D. (2010). Evolution of Transcription Networks — Lessons from Yeasts. Current Biology *20*, R746–R753. https://doi.org/10.1016/j.cub.2010.06.056.
36. Munro, C.A., and Teixeira, M.C. (2022). Yeast pathogenesis and drug resistance: the beauty of the BYeast. FEMS Yeast Research *22*, foac029. https://doi.org/10.1093/femsyr/foac029.
37. Bassilana, M., Puerner, C., and Arkowitz, R.A. (2020). External signal–mediated polarized growth in fungi. Current Opinion in Cell Biology *62*, 150–158. https://doi.org/10.1016/j.ceb.2019.11.001.
38. Ogawa, M., Bisson, L.F., García-Martínez, T., Mauricio, J.C., and Moreno-García, J. (2019). New insights on yeast and filamentous fungus adhesion in a natural co-immobilization system: proposed advances and applications in wine industry. Appl Microbiol Biotechnol *103*, 4723–4731. https://doi.org/10.1007/s00253-019-09870-4.
39. Gognies, S., Belarbi, A., and Ait Barka, E. (2001). Saccharomyces cerevisiae, a potential pathogen towards grapevine, Vitis vinifera. FEMS Microbiology Ecology *37*, 143–150. https://doi.org/10.1111/j.1574-6941.2001.tb00862.x.
40. Stocker-Wörgötter, E. (2008). Metabolic diversity of lichen-forming ascomycetous fungi: culturing, polyketide and shikimatemetabolite production, and PKS genes. Nat. Prod. Rep. *25*, 188–200. https://doi.org/10.1039/B606983P.

41. Hom, E.F.Y., and Murray, A.W. (2014). Niche engineering demonstrates a latent capacity for fungal-algal mutualism. Science *345*, 94–98. https://doi.org/10.1126/science.1253320.
42. Gimeno, C.J., Ljungdahl, P.O., Styles, C.A., and Fink, G.R. (1992). Unipolar cell divisions in the yeast S. cerevisiae lead to filamentous growth: Regulation by starvation and RAS. Cell *68*, 1077–1090. https://doi.org/10.1016/0092-8674(92)90079-R.
43. Engelberg, D., Mimran, A., Martinetto, H., Otto, J., Simchen, G., Karin, M., and Fink, G.R. (1998). Multicellular Stalk-Like Structures in *Saccharomyces cerevisiae*. J Bacteriol *180*, 3992–3996. https://doi.org/10.1128/JB.180.15.3992-3996.1998.
44. Yoneyama, K., Xie, X., Nomura, T., Yoneyama, K., and Bennett, T. (2022). Supra-organismal regulation of strigolactone exudation and plant development in response to rhizospheric cues in rice. Current Biology *32*, 3601-3608.e3. https://doi.org/10.1016/j.cub.2022.06.047.
45. Wheeldon, C.D., Hamon-Josse, M., Lund, H., Yoneyama, K., and Bennett, T. (2022). Environmental strigolactone drives early growth responses to neighboring plants and soil volume in pea. Current Biology *32*, 3593-3600.e3. https://doi.org/10.1016/j.cub.2022.06.063.
46. Cook, C.E., Whichard, L.P., Turner, B., Wall, M.E., and Egley, G.H. (1966). Germination of Witchweed (*Striga lutea* Lour.): Isolation and Properties of a Potent Stimulant. Science *154*, 1189–1190. https://doi.org/10.1126/science.154.3753.1189.
47. Ejeta, G., and Gressel, J. (2007). Integrating New Technologies for Striga Control: Towards Ending the Witch-Hunt (WORLD SCIENTIFIC) https://doi.org/10.1142/6470.
48. Kobae, Y., Kameoka, H., Sugimura, Y., Saito, K., Ohtomo, R., Fujiwara, T., and Kyozuka, J. (2018). Strigolactone Biosynthesis Genes of Rice are Required for the Punctual Entry of Arbuscular Mycorrhizal Fungi into the Roots. Plant and Cell Physiology *59*, 544–553. https://doi.org/10.1093/pcp/pcy001.
49. Kodama, K., Rich, M.K., Yoda, A., Shimazaki, S., Xie, X., Akiyama, K., Mizuno, Y., Komatsu, A., Luo, Y., Suzuki, H., et al. (2022). An ancestral function of strigolactones as symbiotic rhizosphere signals. Nat Commun *13*, 3974. https://doi.org/10.1038/s41467-022-31708-3.
50. Bernabéu-Roda, L.M., López-Ráez, J.A., and Soto, M.J. (2021). Analyzing the Effect of Strigolactones on the Motility Behavior of Rhizobia. In Strigolactones Methods in

Molecular Biology., C. Prandi and F. Cardinale, eds. (Springer US), pp. 91–103. https://doi.org/10.1007/978-1-0716-1429-7_8.

51. Martínez-García, L.B., De Deyn, G.B., Pugnaire, F.I., Kothamasi, D., and Van Der Heijden, M.G.A. (2017). Symbiotic soil fungi enhance ecosystem resilience to climate change. Global Change Biology *23*, 5228–5236. https://doi.org/10.1111/gcb.13785.

52. Belmondo, S., Marschall, R., Tudzynski, P., López Ráez, J.A., Artuso, E., Prandi, C., and Lanfranco, L. (2017). Identification of genes involved in fungal responses to strigolactones using mutants from fungal pathogens. Curr Genet *63*, 201–213. https://doi.org/10.1007/s00294-016-0626-y.

53. Carvalhais, L.C., Rincon-Florez, V.A., Brewer, P.B., Beveridge, C.A., Dennis, P.G., and Schenk, P.M. (2019). The ability of plants to produce strigolactones affects rhizosphere community composition of fungi but not bacteria. Rhizosphere *9*, 18–26. https://doi.org/10.1016/j.rhisph.2018.10.002.

54. Liu, F., Rice, J.H., Lopes, V., Grewal, P., Lebeis, S.L., Hewezi, T., and Staton, M.E. (2020). Overexpression of Strigolactone-Associated Genes Exerts Fine-Tuning Selection on Soybean Rhizosphere Bacterial and Fungal Microbiome. Phytobiomes Journal *4*, 239–251. https://doi.org/10.1094/PBIOMES-01-20-0003-R.

55. López-Ráez, J.A., Shirasu, K., and Foo, E. (2017). Strigolactones in Plant Interactions with Beneficial and Detrimental Organisms: The Yin and Yang. Trends in Plant Science *22*, 527–537. https://doi.org/10.1016/j.tplants.2017.03.011.

56. Zwanenburg, B., and Pospíšil, T. (2013). Structure and Activity of Strigolactones: New Plant Hormones with a Rich Future. Molecular Plant *6*, 38–62. https://doi.org/10.1093/mp/sss141.

57. Austin, S., and Mayer, A. (2020). Phosphate Homeostasis − A Vital Metabolic Equilibrium Maintained Through the INPHORS Signaling Pathway. Front. Microbiol. *11*, 1367. https://doi.org/10.3389/fmicb.2020.01367.

58. O'Neill, E.M., Kaffman, A., Jolly, E.R., and O'Shea, E.K. (1996). Regulation of PHO4 Nuclear Localization by the PHO80-PHO85 Cyclin-CDK Complex. Science *271*, 209–212. https://doi.org/10.1126/science.271.5246.209.

59. Chabert, V., Kim, G.-D., Qiu, D., Liu, G., Michaillat Mayer, L., Jamsheer K, M., Jessen, H.J., and Mayer, A. (2023). Inositol pyrophosphate dynamics reveals control of the yeast

phosphate starvation program through 1,5-IP8 and the SPX domain of Pho81. eLife *12*, RP87956. https://doi.org/10.7554/eLife.87956.

60. Boer, V.M., Crutchfield, C.A., Bradley, P.H., Botstein, D., and Rabinowitz, J.D. (2010). Growth-limiting Intracellular Metabolites in Yeast Growing under Diverse Nutrient Limitations. MBoC *21*, 198–211. https://doi.org/10.1091/mbc.e09-07-0597.

61. Gerasimaitė, R., and Mayer, A. (2016). Enzymes of yeast polyphosphate metabolism: structure, enzymology and biological roles. Biochemical Society Transactions *44*, 234–239. https://doi.org/10.1042/BST20150213.

62. Popova, Y., Thayumanavan, P., Lonati, E., Agrochão, M., and Thevelein, J.M. (2010). Transport and signaling through the phosphate-binding site of the yeast Pho84 phosphate transceptor. Proc. Natl. Acad. Sci. U.S.A. *107*, 2890–2895. https://doi.org/10.1073/pnas.0906546107.

63. Bun-Ya, M., Nishimura, M., Harashima, S., and Oshima, Y. (1991). The PHO84 gene of Saccharomyces cerevisiae encodes an inorganic phosphate transporter. Mol Cell Biol *11*, 3229–3238. https://doi.org/10.1128/mcb.11.6.3229-3238.1991.

64. Wykoff, D.D., Rizvi, A.H., Raser, J.M., Margolin, B., and O'Shea, E.K. (2007). Positive Feedback Regulates Switching of Phosphate Transporters in S. cerevisiae. Molecular Cell *27*, 1005–1013. https://doi.org/10.1016/j.molcel.2007.07.022.

65. Jensen, L.T., Ajua-Alemanji, M., and Culotta, V.C. (2003). The Saccharomyces cerevisiae High Affinity Phosphate Transporter Encoded by PHO84 Also Functions in Manganese Homeostasis. Journal of Biological Chemistry *278*, 42036–42040. https://doi.org/10.1074/jbc.M307413200.

66. Wykoff, D.D., and O'Shea, E.K. (2001). Phosphate transport and sensing in Saccharomyces cerevisiae. Genetics *159*, 1491–1499. https://doi.org/10.1093/genetics/159.4.1491.

67. Lomenick, B., Hao, R., Jonai, N., Chin, R.M., Aghajan, M., Warburton, S., Wang, J., Wu, R.P., Gomez, F., Loo, J.A., et al. (2009). Target identification using drug affinity responsive target stability (DARTS). Proc Natl Acad Sci U S A *106*, 21984–21989. https://doi.org/10.1073/pnas.0910040106.

68. Pedersen, B.P., Kumar, H., Waight, A.B., Risenmay, A.J., Roe-Zurz, Z., Chau, B.H., Schlessinger, A., Bonomi, M., Harries, W., Sali, A., et al. (2013). Crystal structure of a

eukaryotic phosphate transporter. Nature *496*, 533–536. https://doi.org/10.1038/nature12042.

69. Petersson, J., Pattison, J., Kruckeberg, A.L., Berden, J.A., and Persson, B.L. (1999). Intracellular localization of an active green fluorescent protein-tagged Pho84 phosphate permease in Saccharomyces cerevisiae. FEBS Lett *462*, 37–42. https://doi.org/10.1016/s0014-5793(99)01471-4.

70. Qiang, X., Weiss, M., Kogel, K., and Schäfer, P. (2012). *Piriformospora indica* —a mutualistic basidiomycete with an exceptionally large plant host range. Molecular Plant Pathology *13*, 508–518. https://doi.org/10.1111/j.1364-3703.2011.00764.x.

71. Pérez-Alonso, M.-M., Guerrero-Galán, C., Scholz, S.S., Kiba, T., Sakakibara, H., Ludwig-Müller, J., Krapp, A., Oelmüller, R., Vicente-Carbajosa, J., and Pollmann, S. (2020). Harnessing symbiotic plant–fungus interactions to unleash hidden forces from extreme plant ecosystems. Journal of Experimental Botany *71*, 3865–3877. https://doi.org/10.1093/jxb/eraa040.

72. Moonjely, S., Ebert, M., Paton-Glassbrook, D., Noel, Z.A., Roze, L., Shay, R., Watkins, T., and Trail, F. (2023). Update on the state of research to manage Fusarium head blight. Fungal Genetics and Biology *169*, 103829. https://doi.org/10.1016/j.fgb.2023.103829.

73. Zhang, Y., He, J., Jia, L.-J., Yuan, T.-L., Zhang, D., Guo, Y., Wang, Y., and Tang, W.-H. (2016). Cellular Tracking and Gene Profiling of Fusarium graminearum during Maize Stalk Rot Disease Development Elucidates Its Strategies in Confronting Phosphorus Limitation in the Host Apoplast. PLoS Pathog *12*, e1005485. https://doi.org/10.1371/journal.ppat.1005485.

74. Payandeh, J., and Volgraf, M. (2021). Ligand binding at the protein-lipid interface: strategic considerations for drug design. Nat Rev Drug Discov *20*, 710–722. https://doi.org/10.1038/s41573-021-00240-2.

75. Xie, X., Yoneyama, K., and Yoneyama, K. (2010). The Strigolactone Story. Annu. Rev. Phytopathol. *48*, 93–117. https://doi.org/10.1146/annurev-phyto-073009-114453.

76. Perlstein, E.O., Ruderfer, D.M., Roberts, D.C., Schreiber, S.L., and Kruglyak, L. (2007). Genetic basis of individual differences in the response to small-molecule drugs in yeast. Nat Genet *39*, 496–502. https://doi.org/10.1038/ng1991.

77. Beccaccioli, M., Pucci, N., Salustri, M., Scortichini, M., Zaccaria, M., Momeni, B., Loreti, S., Reverberi, M., and Scala, V. (2022). Fungal and bacterial oxylipins are signals for intra- and inter-cellular communication within plant disease. Front. Plant Sci. *13*, 823233. https://doi.org/10.3389/fpls.2022.823233.

78. Deboever, E., Deleu, M., Mongrand, S., Lins, L., and Fauconnier, M.-L. (2020). Plant–Pathogen Interactions: Underestimated Roles of Phyto-oxylipins. Trends in Plant Science *25*, 22–34. https://doi.org/10.1016/j.tplants.2019.09.009.

79. Wang, Y., Mostafa, S., Zeng, W., and Jin, B. (2021). Function and Mechanism of Jasmonic Acid in Plant Responses to Abiotic and Biotic Stresses. IJMS *22*, 8568. https://doi.org/10.3390/ijms22168568.

80. Eng, F., Marin, J.E., Zienkiewicz, K., Gutiérrez-Rojas, M., Favela-Torres, E., and Feussner, I. (2021). Jasmonic acid biosynthesis by fungi: derivatives, first evidence on biochemical pathways and culture conditions for production. PeerJ *9*, e10873. https://doi.org/10.7717/peerj.10873.

81. Yao, H.J., and Tian, S.P. (2005). Effects of a biocontrol agent and methyl jasmonate on postharvest diseases of peach fruit and the possible mechanisms involved. J Appl Microbiol *98*, 941–950. https://doi.org/10.1111/j.1365-2672.2004.02531.x.

82. Jiang, A.-L., Liu, Y.-N., Liu, R., Ren, A., Ma, H.-Y., Shu, L.-B., Shi, L., Zhu, J., and Zhao, M.-W. (2019). Integrated Proteomics and Metabolomics Analysis Provides Insights into Ganoderic Acid Biosynthesis in Response to Methyl Jasmonate in Ganoderma Lucidum. IJMS *20*, 6116. https://doi.org/10.3390/ijms20246116.

83. Tsitsigiannis, D.I., Kowieski, T.M., Zarnowski, R., and Keller, N.P. (2005). Three putative oxylipin biosynthetic genes integrate sexual and asexual development in Aspergillus nidulans. Microbiology *151*, 1809–1821. https://doi.org/10.1099/mic.0.27880-0.

84. Niu, M., Steffan, B.N., Fischer, G.J., Venkatesh, N., Raffa, N.L., Wettstein, M.A., Bok, J.W., Greco, C., Zhao, C., Berthier, E., et al. (2020). Fungal oxylipins direct programmed developmental switches in filamentous fungi. Nat Commun *11*, 5158. https://doi.org/10.1038/s41467-020-18999-0.

85. Kayikci, Ö., and Nielsen, J. (2015). Glucose repression in Saccharomyces cerevisiae. FEMS Yeast Res *15*, fov068. https://doi.org/10.1093/femsyr/fov068.

86. Perez-Nadales, E., Almeida Nogueira, M.F., Baldin, C., Castanheira, S., El Ghalid, M., Grund, E., Lengeler, K., Marchegiani, E., Mehrotra, P.V., Moretti, M., et al. (2014). Fungal model systems and the elucidation of pathogenicity determinants. Fungal Genetics and Biology *70*, 42–67. https://doi.org/10.1016/j.fgb.2014.06.011.

87. Stajich, J.E., Berbee, M.L., Blackwell, M., Hibbett, D.S., James, T.Y., Spatafora, J.W., and Taylor, J.W. (2009). The Fungi. Current Biology *19*, R840–R845. https://doi.org/10.1016/j.cub.2009.07.004.

88. Spatafora, J.W., Aime, M.C., Grigoriev, I.V., Martin, F., Stajich, J.E., and Blackwell, M. (2017). The Fungal Tree of Life: from Molecular Systematics to Genome-Scale Phylogenies. Microbiol Spectr *5*, 5.5.03. https://doi.org/10.1128/microbiolspec.FUNK-0053-2016.

89. Remy, W., Taylor, T.N., Hass, H., and Kerp, H. (1994). Four hundred-million-year-old vesicular arbuscular mycorrhizae. Proc. Natl. Acad. Sci. U.S.A. *91*, 11841–11843. https://doi.org/10.1073/pnas.91.25.11841.

90. Delaux, P.-M., and Schornack, S. (2021). Plant evolution driven by interactions with symbiotic and pathogenic microbes. Science *371*, eaba6605. https://doi.org/10.1126/science.aba6605.

91. Walder, F., Boller, T., Wiemken, A., and Courty, P.-E. (2016). Regulation of plants' phosphate uptake in common mycorrhizal networks: Role of intraradical fungal phosphate transporters. Plant Signaling & Behavior *11*, e1131372. https://doi.org/10.1080/15592324.2015.1131372.

92. Miyagi, M., Wilson, R., Saigusa, D., Umeda, K., Saijo, R., Hager, C.L., Li, Y., McCormick, T., and Ghannoum, M.A. (2020). Indole-3-acetic acid synthesized through the indole-3-pyruvate pathway promotes Candida tropicalis biofilm formation. PLoS ONE *15*, e0244246. https://doi.org/10.1371/journal.pone.0244246.

93. Rao, R.P., Hunter, A., Kashpur, O., and Normanly, J. (2010). Aberrant Synthesis of Indole-3-Acetic Acid in *Saccharomyces cerevisiae* Triggers Morphogenic Transition, a Virulence Trait of Pathogenic Fungi. Genetics *185*, 211–220. https://doi.org/10.1534/genetics.109.112854.

94. Dor, E., Yoneyama, K., Wininger, S., Kapulnik, Y., Yoneyama, K., Koltai, H., Xie, X., and Hershenhorn, J. (2011). Strigolactone deficiency confers resistance in tomato line SL-

ORT1 to the parasitic weeds Phelipanche and Orobanche spp. Phytopathology *101*, 213–222. https://doi.org/10.1094/PHYTO-07-10-0184.

95. Desmarini, D., Lev, S., Furkert, D., Crossett, B., Saiardi, A., Kaufman-Francis, K., Li, C., Sorrell, T.C., Wilkinson-White, L., Matthews, J., et al. (2020). IP $_7$ -SPX Domain Interaction Controls Fungal Virulence by Stabilizing Phosphate Signaling Machinery. mBio *11*, e01920-20. https://doi.org/10.1128/mBio.01920-20.

96. Joska, T.M., Mashruwala, A., Boyd, J.M., and Belden, W.J. (2014). A universal cloning method based on yeast homologous recombination that is simple, efficient, and versatile. J Microbiol Methods *100*, 46–51. https://doi.org/10.1016/j.mimet.2013.11.013.

97. Alberti, S., Gitler, A.D., and Lindquist, S. (2007). A suite of Gateway cloning vectors for high-throughput genetic analysis in Saccharomyces cerevisiae. Yeast *24*, 913–919. https://doi.org/10.1002/yea.1502.

98. Bean, B.D.M., Whiteway, M., and Martin, V.J.J. (2022). The MyLO CRISPR-Cas9 toolkit: a markerless yeast localization and overexpression CRISPR-Cas9 toolkit. G3 Genes|Genomes|Genetics *12*, jkac154. https://doi.org/10.1093/g3journal/jkac154.

99. Biss, M., Hanna, M.D., and Xiao, W. (2014). Isolation of yeast nucleic acids. Methods Mol Biol *1163*, 15–21. https://doi.org/10.1007/978-1-4939-0799-1_2.

100. Babraham Bioinformatics - FastQC A Quality Control tool for High Throughput Sequence Data https://www.bioinformatics.babraham.ac.uk/projects/fastqc/.

101. Kim, D., Paggi, J.M., Park, C., Bennett, C., and Salzberg, S.L. (2019). Graph-based genome alignment and genotyping with HISAT2 and HISAT-genotype. Nat Biotechnol *37*, 907–915. https://doi.org/10.1038/s41587-019-0201-4.

102. Patro, R., Duggal, G., Love, M.I., Irizarry, R.A., and Kingsford, C. (2017). Salmon provides fast and bias-aware quantification of transcript expression. Nat Methods *14*, 417–419. https://doi.org/10.1038/nmeth.4197.

103. R Core Team (2023). R: A Language and Environment for Statistical Computing (R Foundation for Statistical Computing).

104. Love, M.I., Huber, W., and Anders, S. (2014). Moderated estimation of fold change and dispersion for RNA-seq data with DESeq2. Genome Biology *15*, 550. https://doi.org/10.1186/s13059-014-0550-8.

105. Wickham, H. (2016). ggplot2: Elegant Graphics for Data Analysis (Springer-Verlag New York).
106. Vardi, N., Levy, S., Gurvich, Y., Polacheck, T., Carmi, M., Jaitin, D., Amit, I., and Barkai, N. (2014). Sequential feedback induction stabilizes the phosphate starvation response in budding yeast. Cell Rep *9*, 1122–1134. https://doi.org/10.1016/j.celrep.2014.10.002.
107. Roberts, G.G., and Hudson, A.P. (2006). Transcriptome profiling of Saccharomyces cerevisiae during a transition from fermentative to glycerol-based respiratory growth reveals extensive metabolic and structural remodeling. Mol Genet Genomics *276*, 170–186. https://doi.org/10.1007/s00438-006-0133-9.
108. Gu, Z., Eils, R., and Schlesner, M. (2016). Complex heatmaps reveal patterns and correlations in multidimensional genomic data. Bioinformatics *32*, 2847–2849. https://doi.org/10.1093/bioinformatics/btw313.
109. Toh-E, A., and Oshima, Y. (1974). Characterization of a dominant, constitutive mutation, PHOO, for the repressible acid phosphatase synthesis in Saccharomyces cerevisiae. J Bacteriol *120*, 608–617. https://doi.org/10.1128/jb.120.2.608-617.1974.
110. Weir, M., and Keeney, J.B. (2014). PCR mutagenesis and gap repair in yeast. Methods Mol Biol *1205*, 29–35. https://doi.org/10.1007/978-1-4939-1363-3_3.
111. Dick, W.A., and Tabatabai, M.A. (1977). Determination of Orthophosphate in Aqueous Solutions Containing Labile Organic and Inorganic Phosphorus Compounds. Journal of Environmental Quality *6*, 82–85. https://doi.org/10.2134/jeq1977.00472425000600010018x.
112. Kielkopf, C.L., Bauer, W., and Urbatsch, I.L. (2020). Bradford Assay for Determining Protein Concentration. Cold Spring Harb Protoc *2020*, pdb.prot102269. https://doi.org/10.1101/pdb.prot102269.
113. Mülleder, M., Capuano, F., Pir, P., Christen, S., Sauer, U., Oliver, S.G., and Ralser, M. (2012). A prototrophic deletion mutant collection for yeast metabolomics and systems biology. Nat Biotechnol *30*, 1176–1178. https://doi.org/10.1038/nbt.2442.
114. Gietz, R.D., and Woods, R.A. (2006). Yeast transformation by the LiAc/SS Carrier DNA/PEG method. Methods Mol Biol *313*, 107–120. https://doi.org/10.1385/1-59259-958-3:107.

115. Fuhrer, T., Heer, D., Begemann, B., and Zamboni, N. (2011). High-throughput, accurate mass metabolome profiling of cellular extracts by flow injection-time-of-flight mass spectrometry. Anal Chem *83*, 7074–7080. https://doi.org/10.1021/ac201267k.
116. Kanehisa, M., Furumichi, M., Sato, Y., Kawashima, M., and Ishiguro-Watanabe, M. (2023). KEGG for taxonomy-based analysis of pathways and genomes. Nucleic Acids Research *51*, D587–D592. https://doi.org/10.1093/nar/gkac963.
117. Camacho, C., Coulouris, G., Avagyan, V., Ma, N., Papadopoulos, J., Bealer, K., and Madden, T.L. (2009). BLAST+: architecture and applications. BMC Bioinformatics *10*, 421. https://doi.org/10.1186/1471-2105-10-421.
118. UniProt Consortium (2021). UniProt: the universal protein knowledgebase in 2021. Nucleic Acids Res *49*, D480–D489. https://doi.org/10.1093/nar/gkaa1100.
119. Basenko, E.Y., Pulman, J.A., Shanmugasundram, A., Harb, O.S., Crouch, K., Starns, D., Warrenfeltz, S., Aurrecoechea, C., Stoeckert, C.J., Kissinger, J.C., et al. (2018). FungiDB: An Integrated Bioinformatic Resource for Fungi and Oomycetes. J Fungi (Basel) *4*, 39. https://doi.org/10.3390/jof4010039.
120. Edgar, R.C. (2004). MUSCLE: multiple sequence alignment with high accuracy and high throughput. Nucleic Acids Res *32*, 1792–1797. https://doi.org/10.1093/nar/gkh340.
121. Stamatakis, A. (2014). RAxML version 8: a tool for phylogenetic analysis and post-analysis of large phylogenies. Bioinformatics *30*, 1312–1313. https://doi.org/10.1093/bioinformatics/btu033.
122. Yu, G., Lam, T.T.-Y., Zhu, H., and Guan, Y. (2018). Two Methods for Mapping and Visualizing Associated Data on Phylogeny Using Ggtree. Mol Biol Evol *35*, 3041–3043. https://doi.org/10.1093/molbev/msy194.
123. Wagih, O. (2017). ggseqlogo: a versatile R package for drawing sequence logos. Bioinformatics *33*, 3645–3647. https://doi.org/10.1093/bioinformatics/btx469.
124. Waterhouse, A., Bertoni, M., Bienert, S., Studer, G., Tauriello, G., Gumienny, R., Heer, F.T., de Beer, T.A.P., Rempfer, C., Bordoli, L., et al. (2018). SWISS-MODEL: homology modelling of protein structures and complexes. Nucleic Acids Res *46*, W296–W303. https://doi.org/10.1093/nar/gky427.
125. Schrödinger, LLC (2015). The PyMOL Molecular Graphics System, Version 1.8.

126. Jumper, J., Evans, R., Pritzel, A., Green, T., Figurnov, M., Ronneberger, O., Tunyasuvunakool, K., Bates, R., Žídek, A., Potapenko, A., et al. (2021). Highly accurate protein structure prediction with AlphaFold. Nature *596*, 583–589. https://doi.org/10.1038/s41586-021-03819-2.

127. Varadi, M., Anyango, S., Deshpande, M., Nair, S., Natassia, C., Yordanova, G., Yuan, D., Stroe, O., Wood, G., Laydon, A., et al. (2022). AlphaFold Protein Structure Database: massively expanding the structural coverage of protein-sequence space with high-accuracy models. Nucleic Acids Research *50*, D439–D444. https://doi.org/10.1093/nar/gkab1061.

128. Eberhardt, J., Santos-Martins, D., Tillack, A.F., and Forli, S. (2021). AutoDock Vina 1.2.0: New Docking Methods, Expanded Force Field, and Python Bindings. J. Chem. Inf. Model. *61*, 3891–3898. https://doi.org/10.1021/acs.jcim.1c00203.

129. Laskowski, R.A., and Swindells, M.B. (2011). LigPlot+: Multiple Ligand–Protein Interaction Diagrams for Drug Discovery. J. Chem. Inf. Model. *51*, 2778–2786. https://doi.org/10.1021/ci200227u.

130. Fungal rDNA (D1/D2) PCR Kit Fast.

131. White, T., Bruns, T., Lee, S., Taylor, J., Innis, M., Gelfand, D., and Sninsky, J. (1990). Amplification and Direct Sequencing of Fungal Ribosomal RNA Genes for Phylogenetics. In Pcr Protocols: a Guide to Methods and Applications, pp. 315–322.

132. Sugiura, Y., Akiyama, R., Tanaka, S., Yano, K., Kameoka, H., Marui, S., Saito, M., Kawaguchi, M., Akiyama, K., and Saito, K. (2020). Myristate can be used as a carbon and energy source for the asymbiotic growth of arbuscular mycorrhizal fungi. Proceedings of the National Academy of Sciences *117*, 25779–25788. https://doi.org/10.1073/pnas.2006948117.

133. Correll, J.C. (1987). Nitrate Nonutilizing Mutants of Fusarium oxysporum and Their Use in Vegetative Compatibility Tests. Phytopathology *77*. https://doi.org/10.1094/Phyto-77-1640.

134. Peng, D., and Tarleton, R. (2015). EuPaGDT: a web tool tailored to design CRISPR guide RNAs for eukaryotic pathogens. Microb Genom *1*, e000033. https://doi.org/10.1099/mgen.0.000033.

135. Schneider, C.A., Rasband, W.S., and Eliceiri, K.W. (2012). NIH Image to ImageJ: 25 years of image analysis. Nat Methods *9*, 671–675. https://doi.org/10.1038/nmeth.2089.

Figure 1

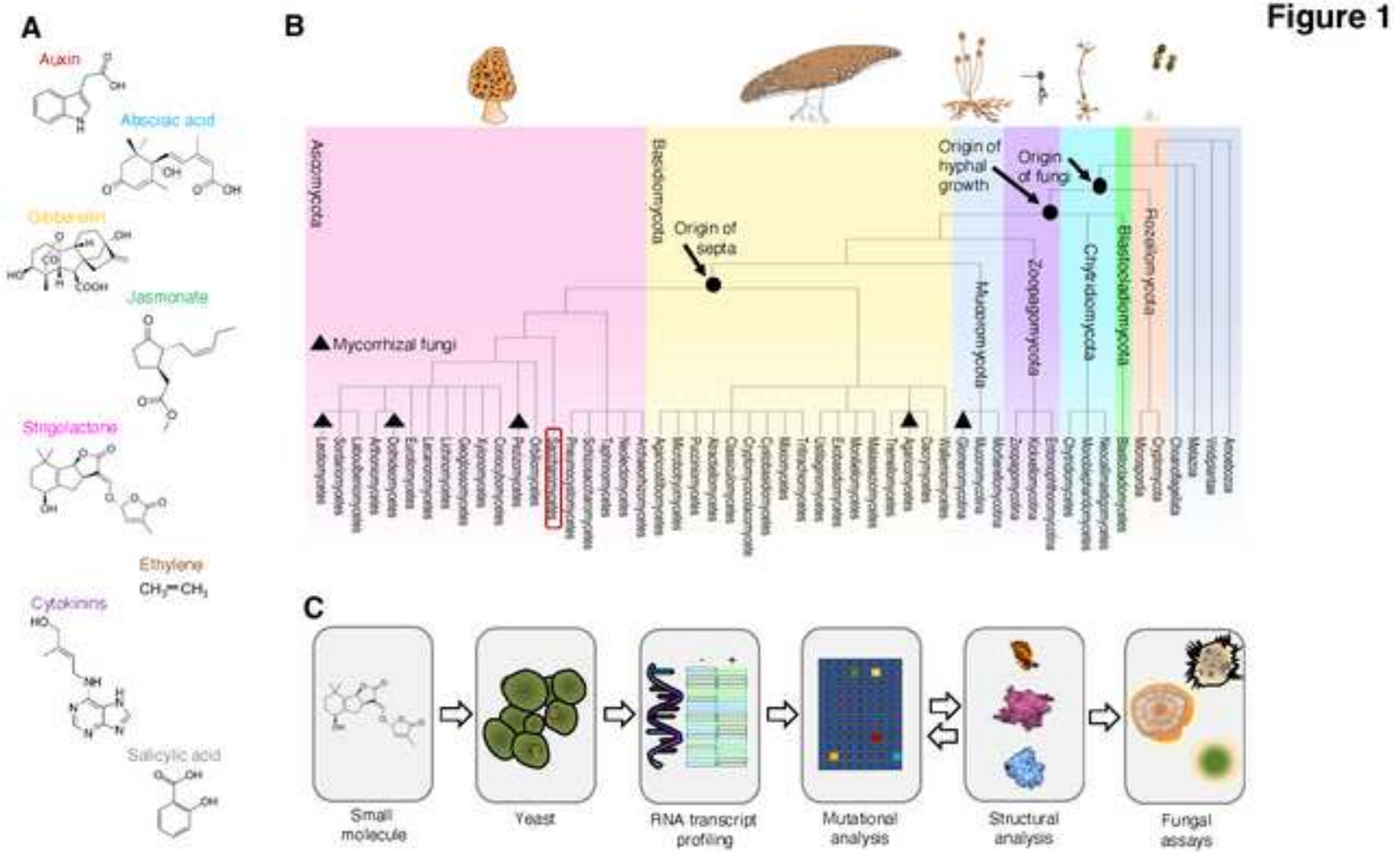

Figure 1

Figure 2

Click here to access/download;Figure;Fig2.TIF

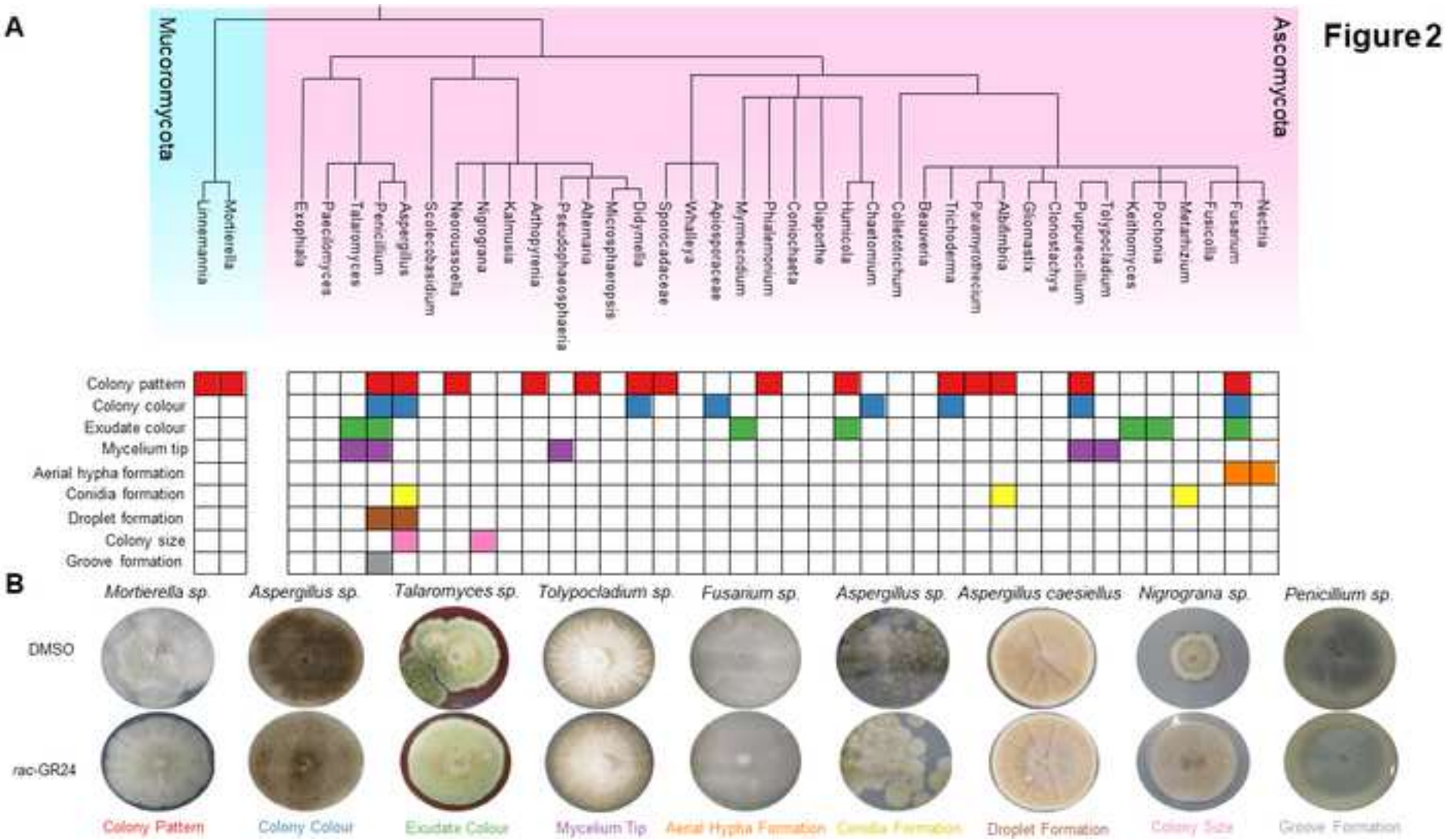

Figure 2

Figure 3

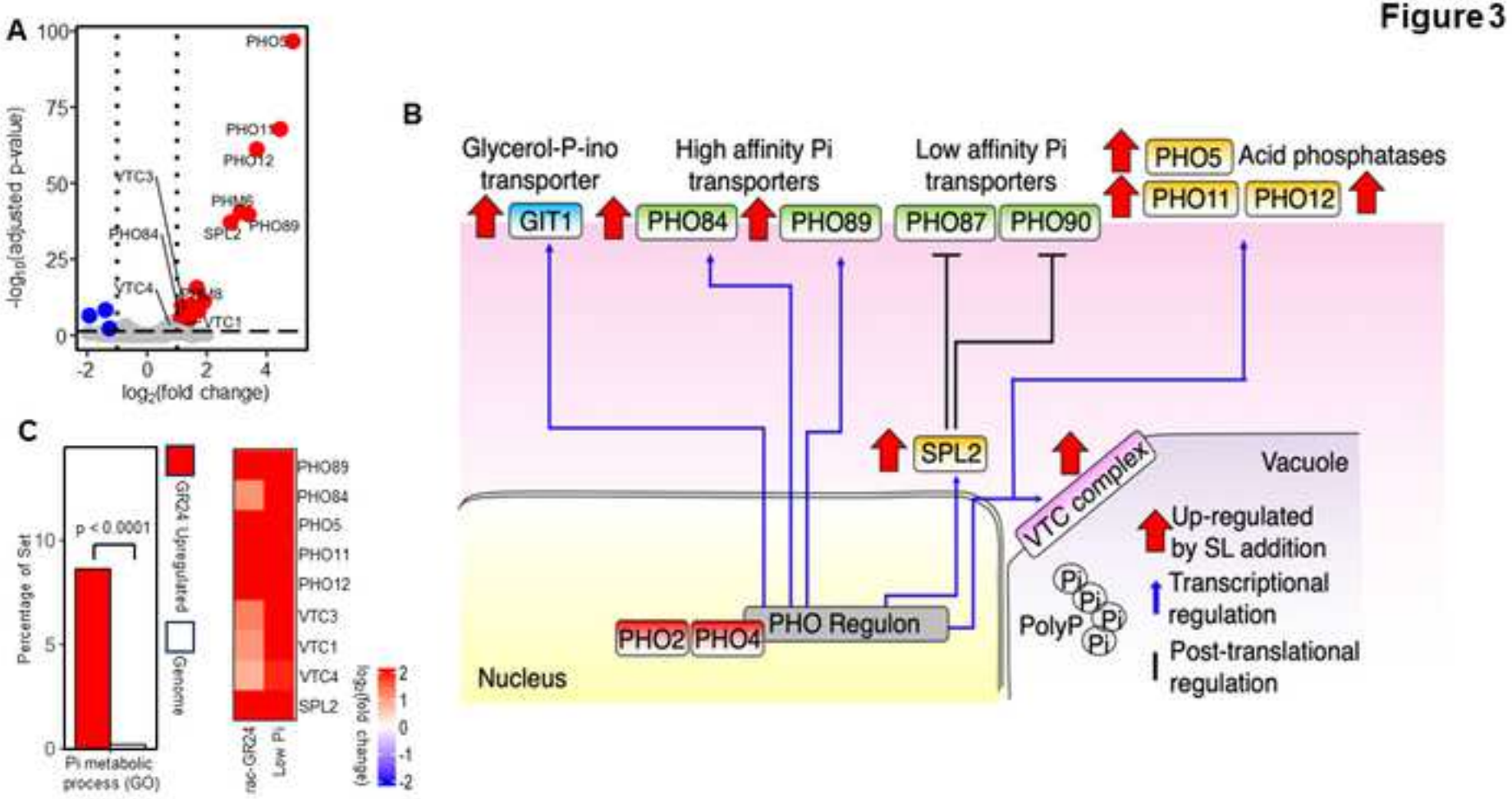

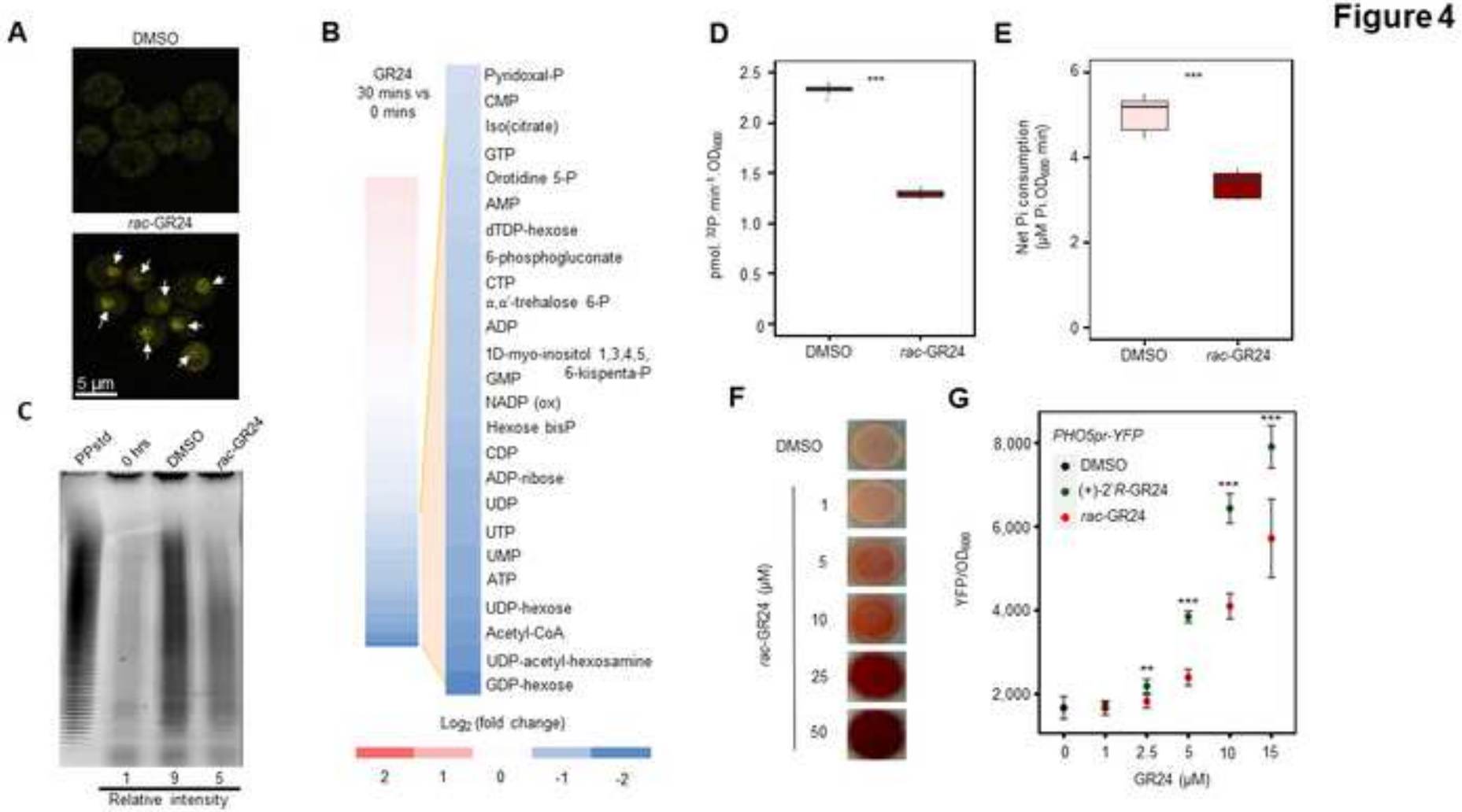

Figure 4

Figure 5

Click here to access/download;Figure;Fig5.TIF

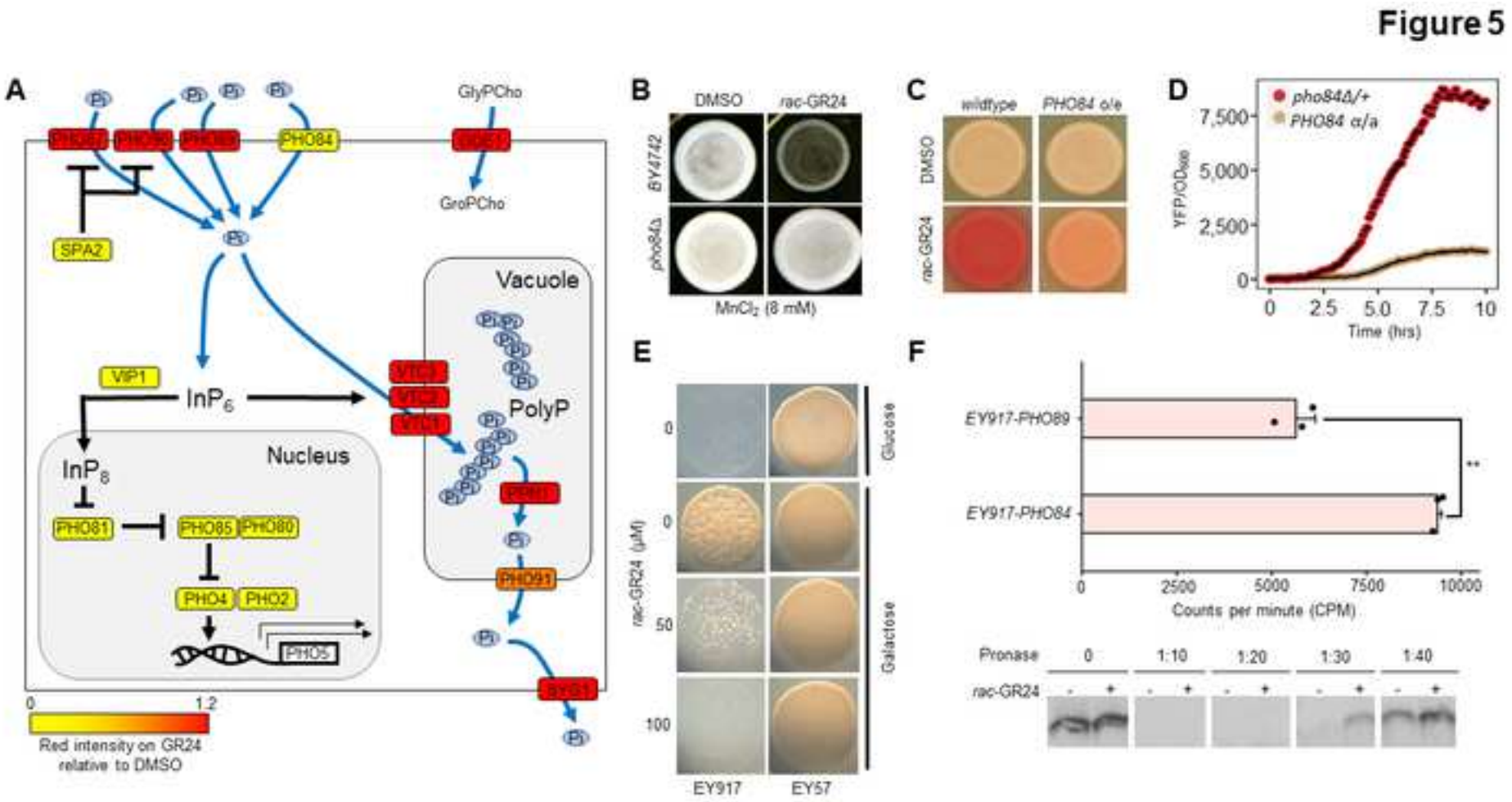

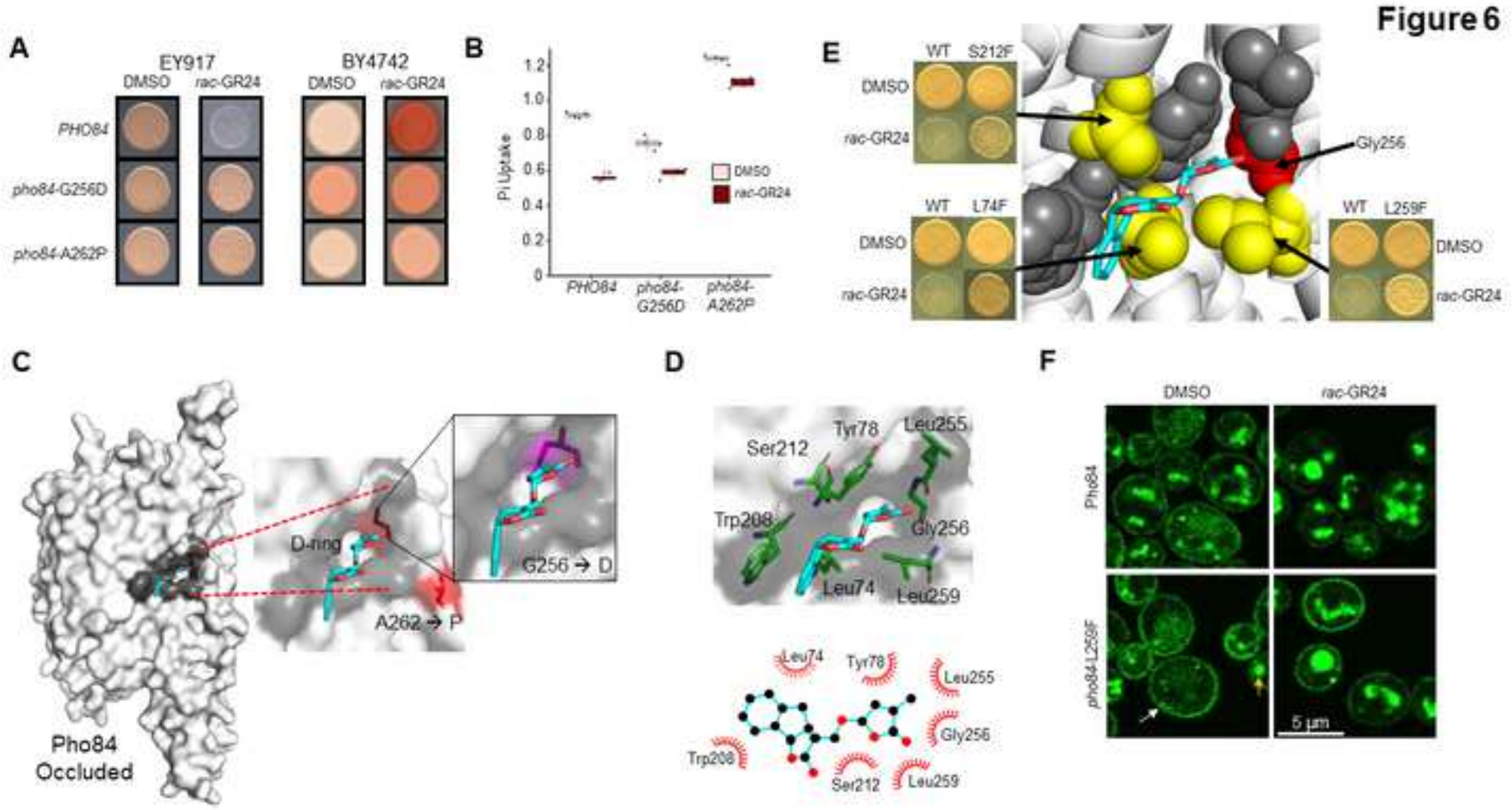

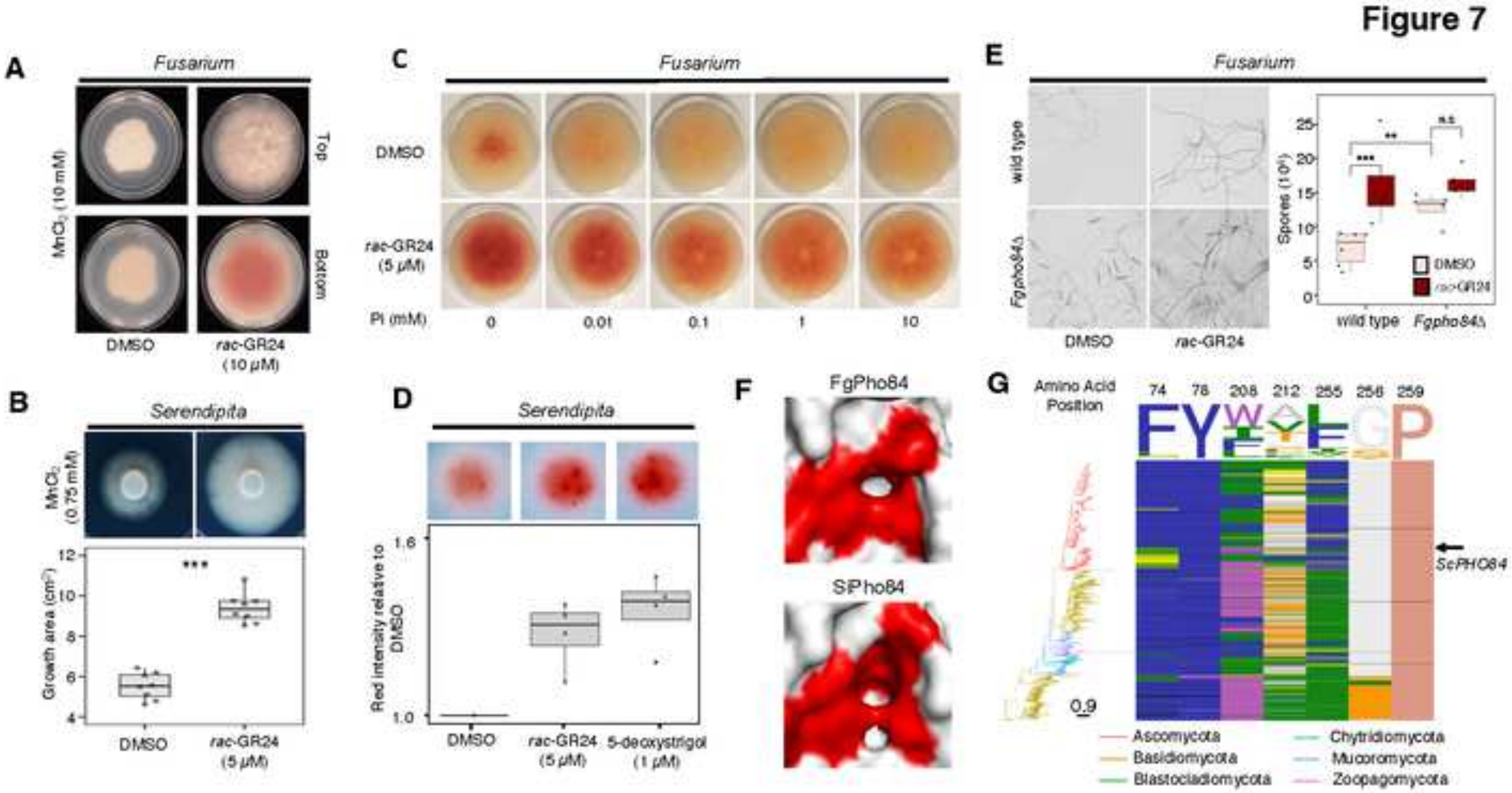

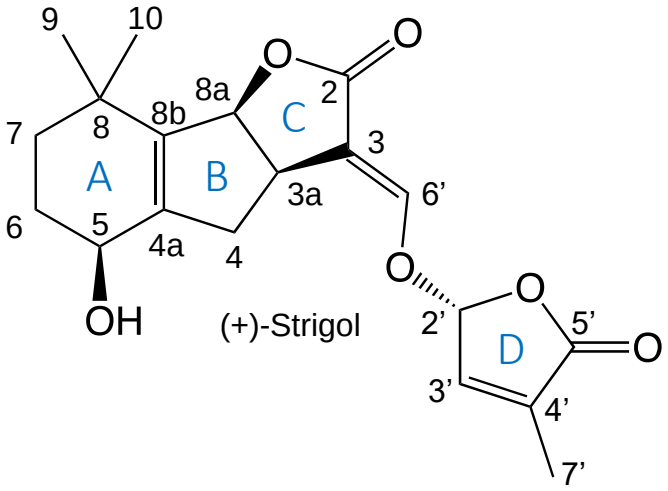

rac-GR24 isomers

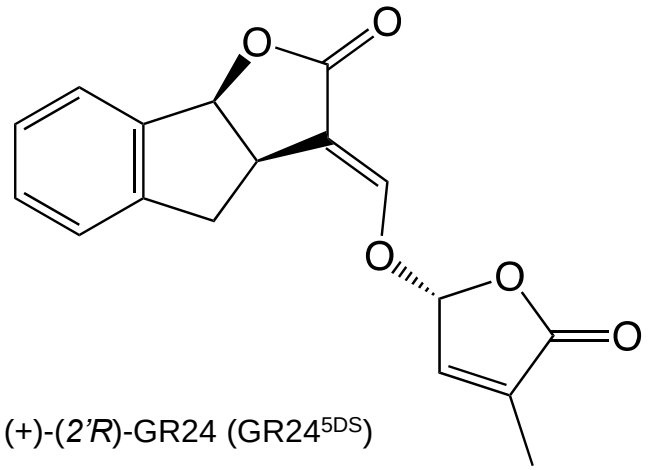

(+)-(*2'R*)-GR24 (GR24^{5DS})

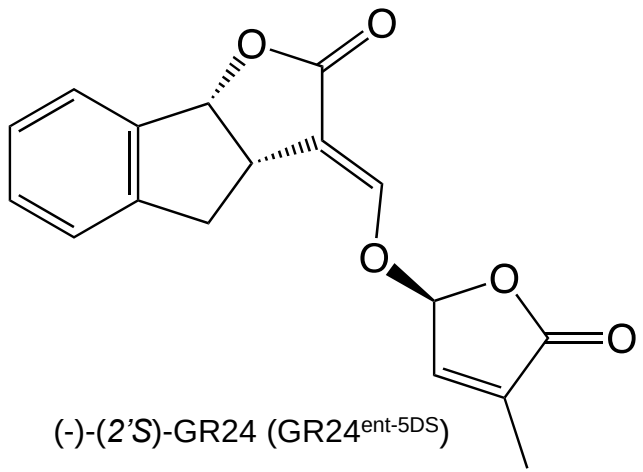

(-)-(*2'S*)-GR24 (GR24$^{ent\text{-}5DS}$)

Figure S1. Structures of strigolactones. Upper panel. Over 20 plant-derived strigolactone like molecules (SLs) have been characterized from root exudates. Canonical SLs share an overall structure which includes a three annulated ABC ring scaffold connected to a butenolide ring through an enol ether linkage. Based on stereochemistry around the BC rings two major SL families, (+)-Strigol and (−)-Orobanchol exist. With respect to the D-ring, all natural SLs have the same *2'-R* stereochemistry (*5DS*). However, artificially synthesized SLs such as *rac*-GR24 are a racemic mixture of *2'-R* and *2'-S* sterioisomers (*ent-5DS*).

A

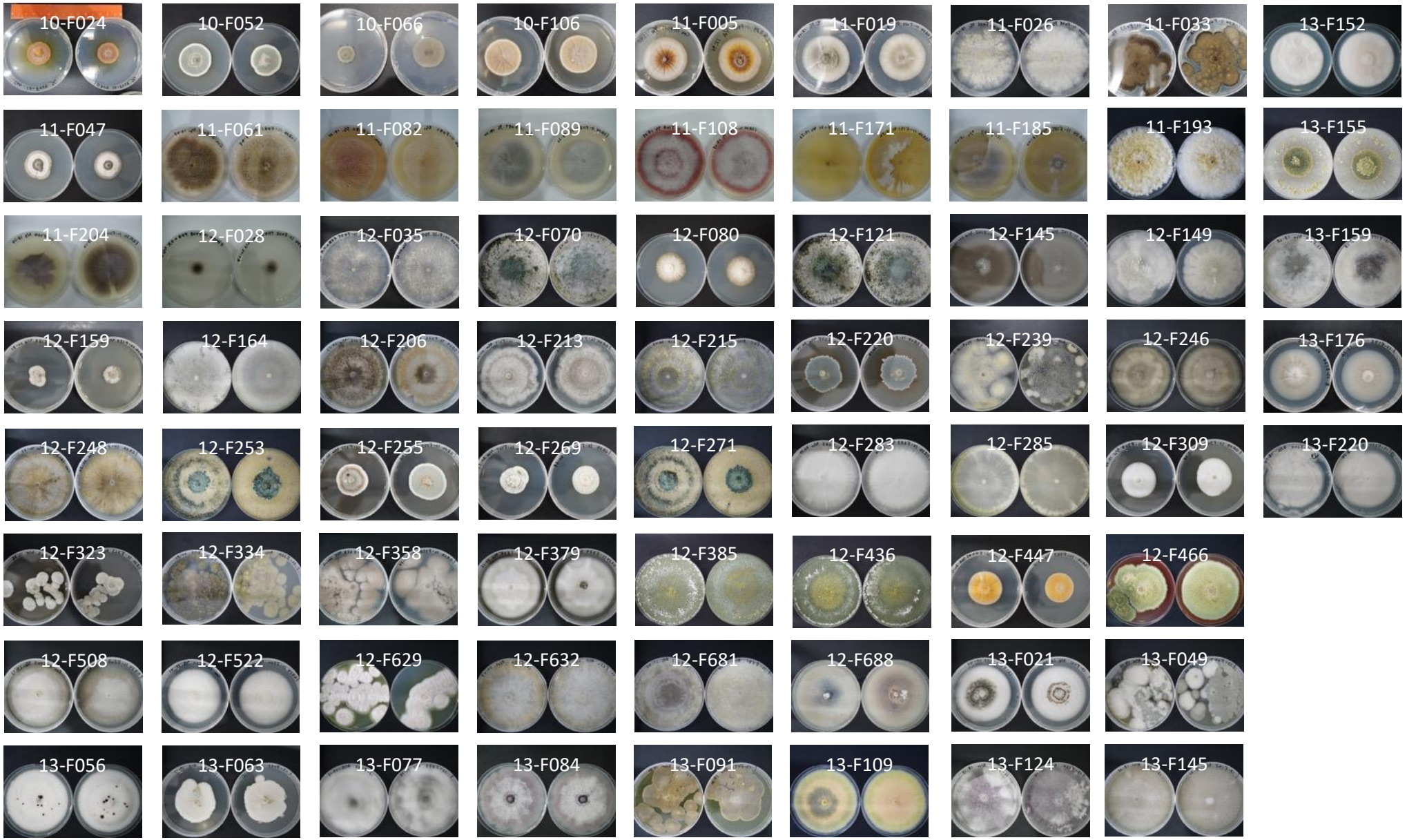

Figure S2. Response of naturally occurring fungi to *rac*-GR24. (**A**) Compilation of 69 naturally occurring soil fungi which showed a response to *rac*-GR24. Each image contains fungi grown on mock media (left) and fungi treated with *rac*-GR24 (right). (**B**) Compilation of 155 naturally occurring soil fungi which showed no response to *rac*-GR24. Each image contains fungi grown on mock media (left) and fungi treated with *rac*-GR24 (right).

Figure S2B


10-F017
11-F020
11-F032
10-F038
11-F042
10-F058
10-F059
11-F068
11-F072
11-F075
11-F083
10-F153
10-F161
10-F168
10-F211
10-F254
10-F259
11-F041
11-F101
11-F115
11-F129
11-F143
11-F178
11-F192
11-F211
11-F212
11-F218
11-F224
11-F225
11-F232
11-F238
11-F239
11-F246
11-F260
11-F267
11-F274
11-F281
11-F288
11-F295
12-F014
12-F021
12-F025
12-F042
12-F056
12-F063
12-F066
12-F074
12-F083
12-F084
12-F091
12-F094
12-F110
12-F131
12-F152
12-F155
12-F162
12-F165
12-F166
12-F172
12-F176
12-F180
12-F180
12-F187
12-F194
12-F214
12-F224
12-F234
12-F262
12-F290
12-F302
12-F316
12-F330
12-F372
12-F405
12-F412
12-F419
12-F433
12-F440
12-F454
12-F458
12-F461
12-F471
12-F475
12-F501
12-F505
12-F513
12-F515
12-F516
12-F521
12-F524

Figure 2B con't

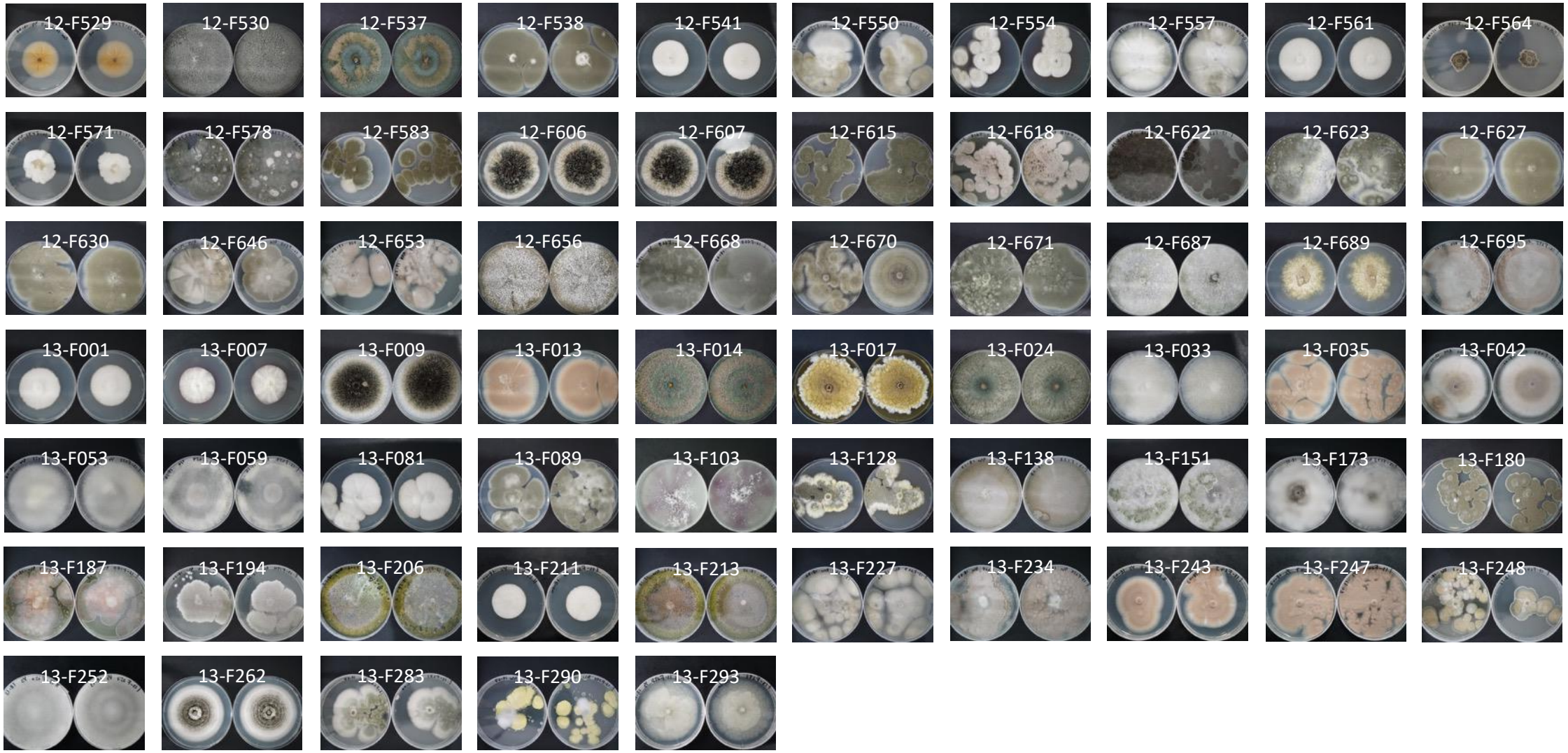

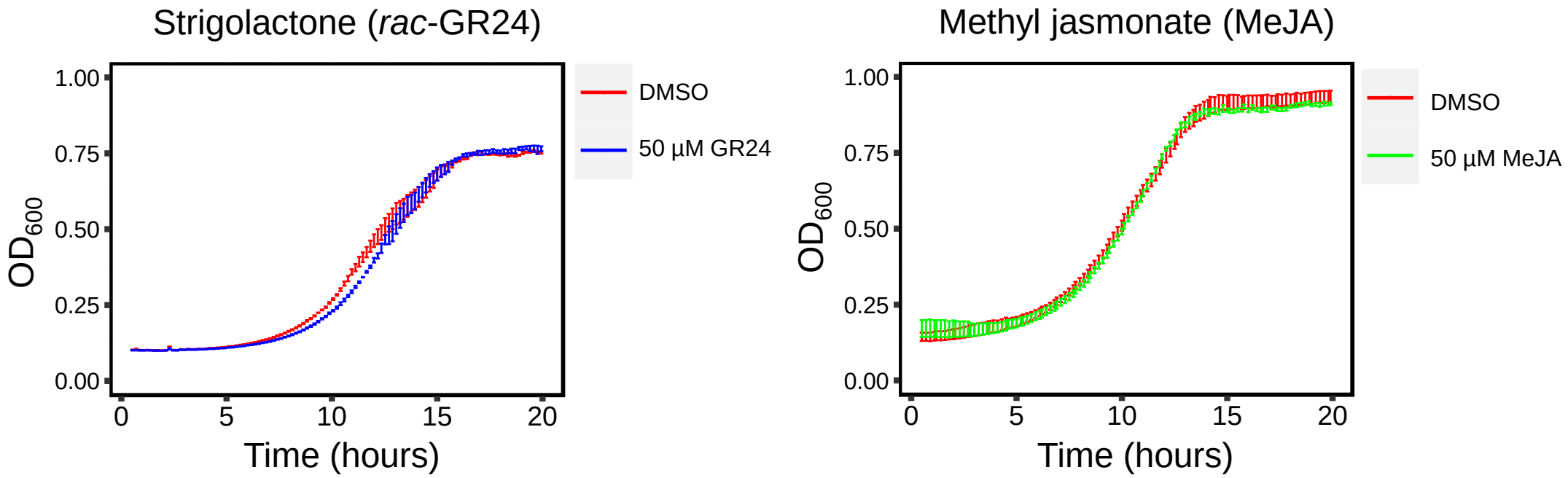

Figure S3. Growth of yeast on strigolactone or methyl jasmonate. Two independent experiments were performed in each case where BY4742 was grown overnight in YPD and then resuspended in fresh YPD media at an OD_{600} ~ 0.12, supplemented with either DMSO or 50 µM GR24 (**a**) or 50 mM MeJA (b) and further grown further for ~ 20 hrs. OD_{600} measurements were made using a plate reader (TECAN) whilst maintaining the cultures at 30˚C.

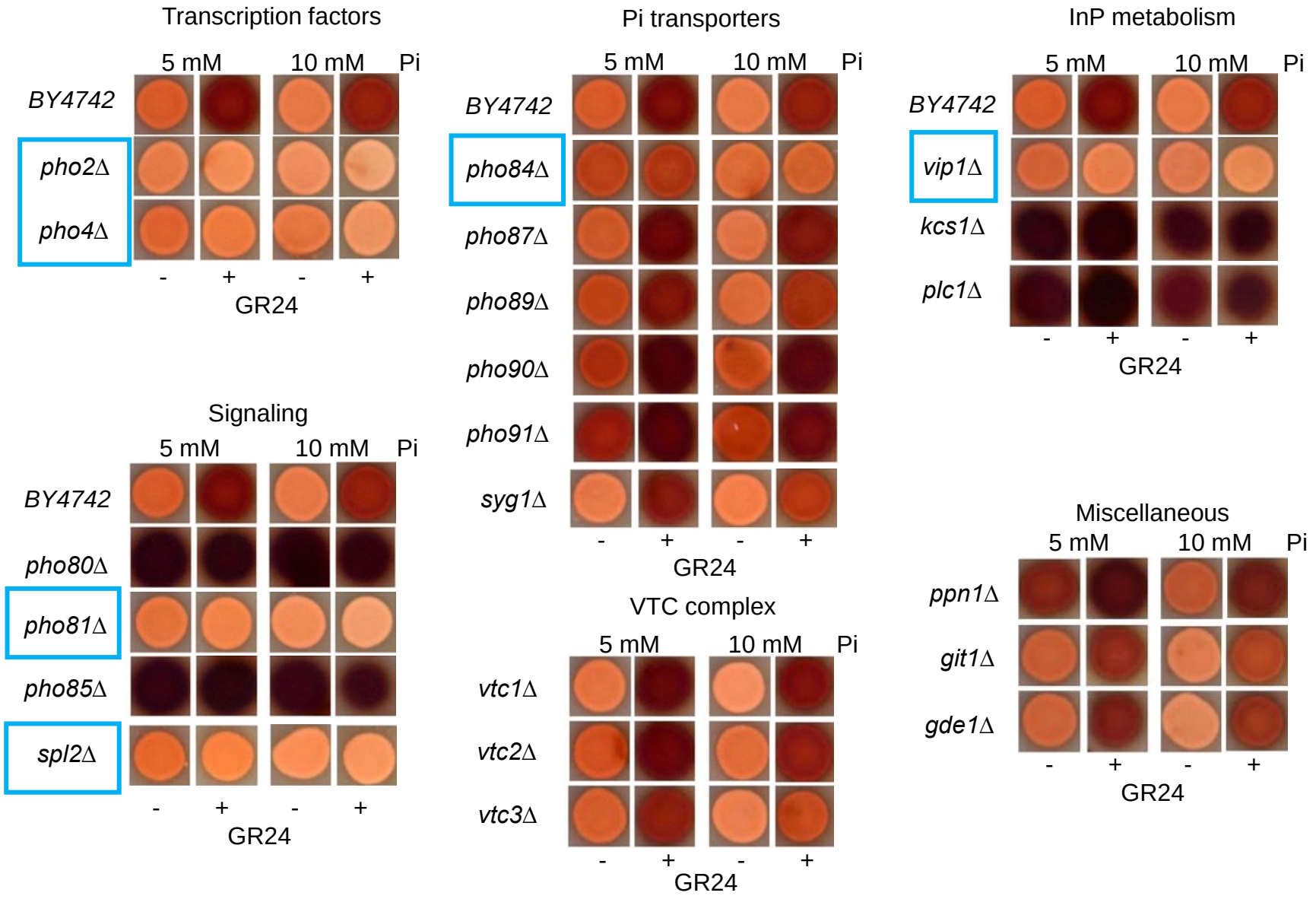

Red intensity on GR24 relative to DMSO

Genotype	5 mM Pi	10 mM Pi
BY4742	1.368	1.384
pho2Δ	0.966	0.935
pho4Δ	0.940	0.888
pho80Δ	1.018	0.902
pho81Δ	0.960	0.935
pho85Δ	0.997	0.884
spl2Δ	0.923	0.971
pho84Δ	1.071	1.007
pho87Δ	1.420	1.453
pho89Δ	1.204	1.266
pho90Δ	1.228	1.152
pho91Δ	1.102	1.072
syg1Δ	1.370	1.310
vtc1Δ	1.496	1.567
vtc2Δ	1.290	1.323
vtc3Δ	1.236	1.249
vip1Δ	0.930	0.963
kcs1Δ	1.183	0.993
plc1Δ	0.961	0.845
ppn1Δ	1.051	1.205
git1Δ	1.182	1.285
gde1Δ	1.252	1.376

Figure S4. Acid phosphatase colony assays of wild type BY4742 and a *PHO* regulon gene knockout mutants. Cells were spotted onto 5 or 10 mM Pi concentrations with or without the addition of 50 µM GR24. The darker the red colony color the more acid phosphatase activity. Some knockout strains (*pho80Δ, pho85Δ, kcs1Δ, plc1Δ*) are not informative for chemical epistasis with GR24 because they are constitutive for acid phosphatase activity on the mock DMSO control. Mutants with reduced GR24 responsiveness compared to wild type are outlined in blue.

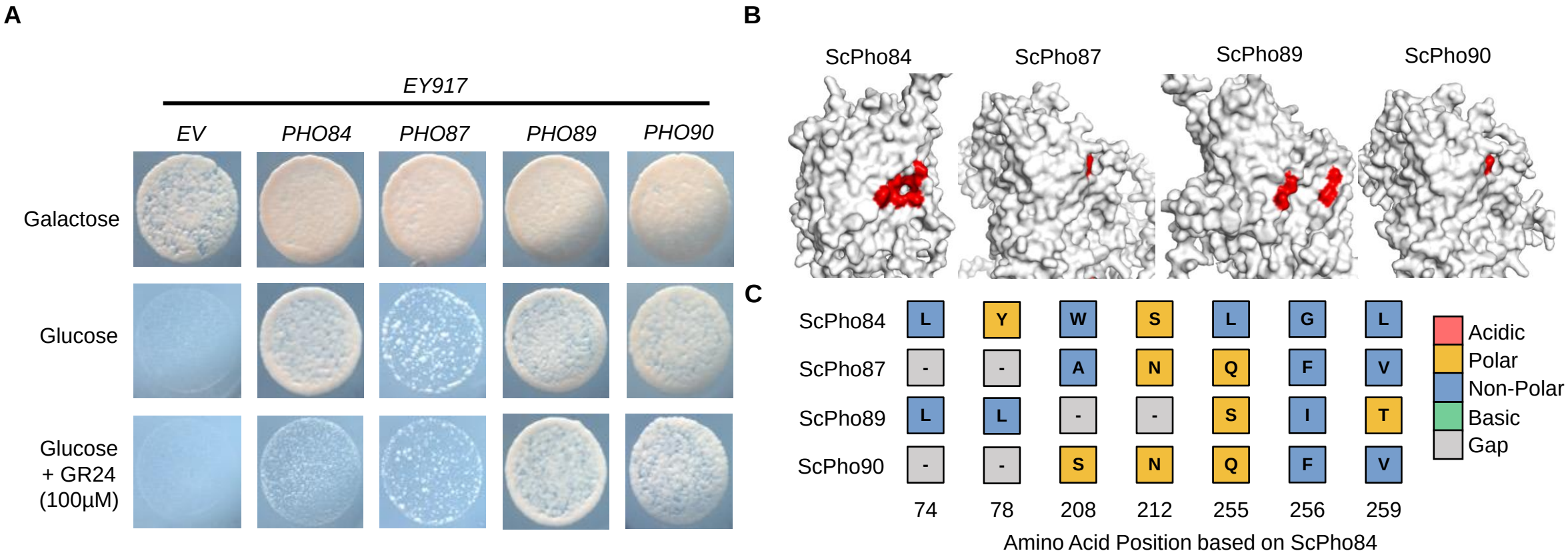

Figure S5. SL specifically inhibits PHO84's phosphate transport activity. A. The EY917 strain is deleted for five Pi transporters (*pho84*Δ*, pho87*Δ*, pho89*Δ*, pho90*Δ*, pho91*Δ) and carries a *PHO* transporter gene under the control of a *GAL1* promoter making Pi transport and viability dependent on galactose [Wykoff & O'Shea, 2001]. On glucose, transporter expression from the *GAL1* promoter is turned off. Growth assay of the EY917 transformed strains on either 2% galactose or 2% glucose ± GR24. EY917 strains were transformed with high-copy plasmids carrying either *PHO84* (*p5587-PHO84*), *PHO87* (*p5587-PHO87*), *PHO89* (*p5819-PHO89*), *PHO90* (*p5819-PHO90*), or the empty vector (*p5587-EV*). EY917 transformed with *PHO87* grows poorly on glucose because it encodes an alkaline phosphatase that activates poorly on slightly acidic yeast media. **B.** Homology models of the four major Pi transporters in yeast. Red represents amino acids identified as being important in Pho84 recognition of GR24. As noted, Pho87, Pho89 and Pho90 models do not show a binding pocket. **C**. Comparisons of amino acid sequences of regions with the Pho84 pocket domain. Ten key amino acids identified by LigPlot+ as interacting with GR24 binding are marked with arrows.

A Phylogeny of methyl jasmonate responsive fungi

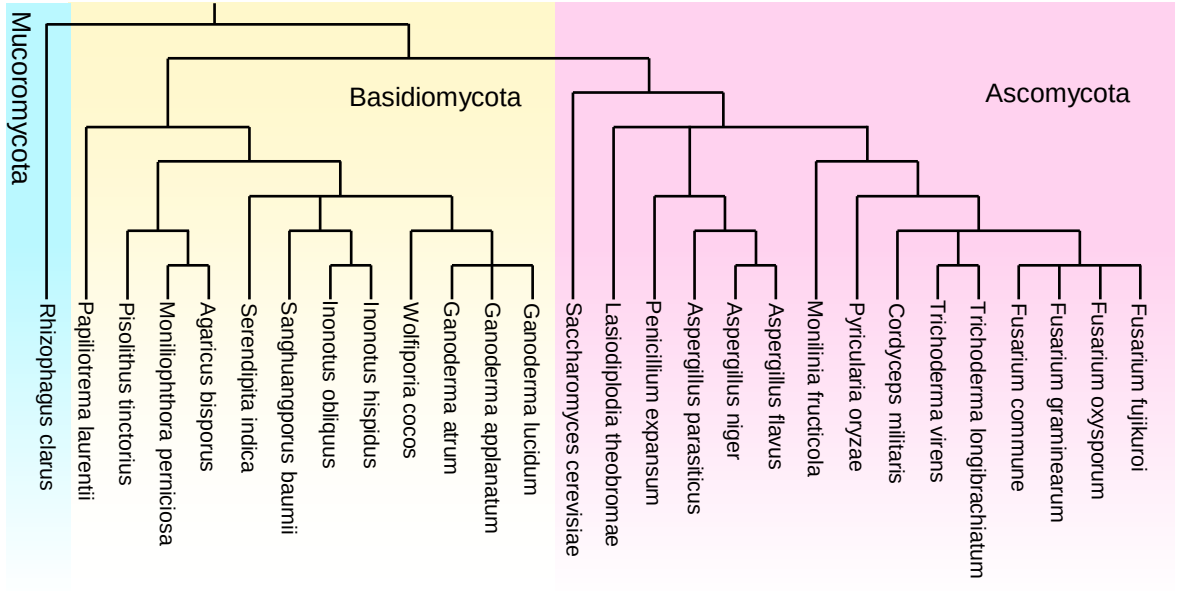

B Methyl jasmonate transcriptome analysis

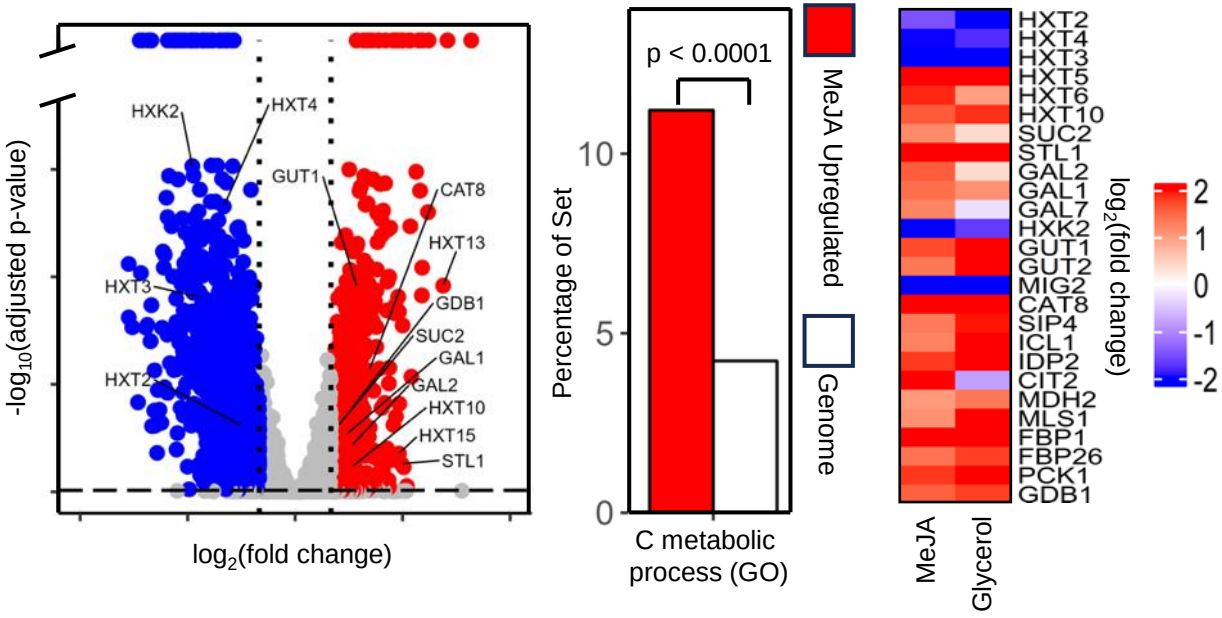

C Placement of methyl jasmonate regulated genes in sugar regulon

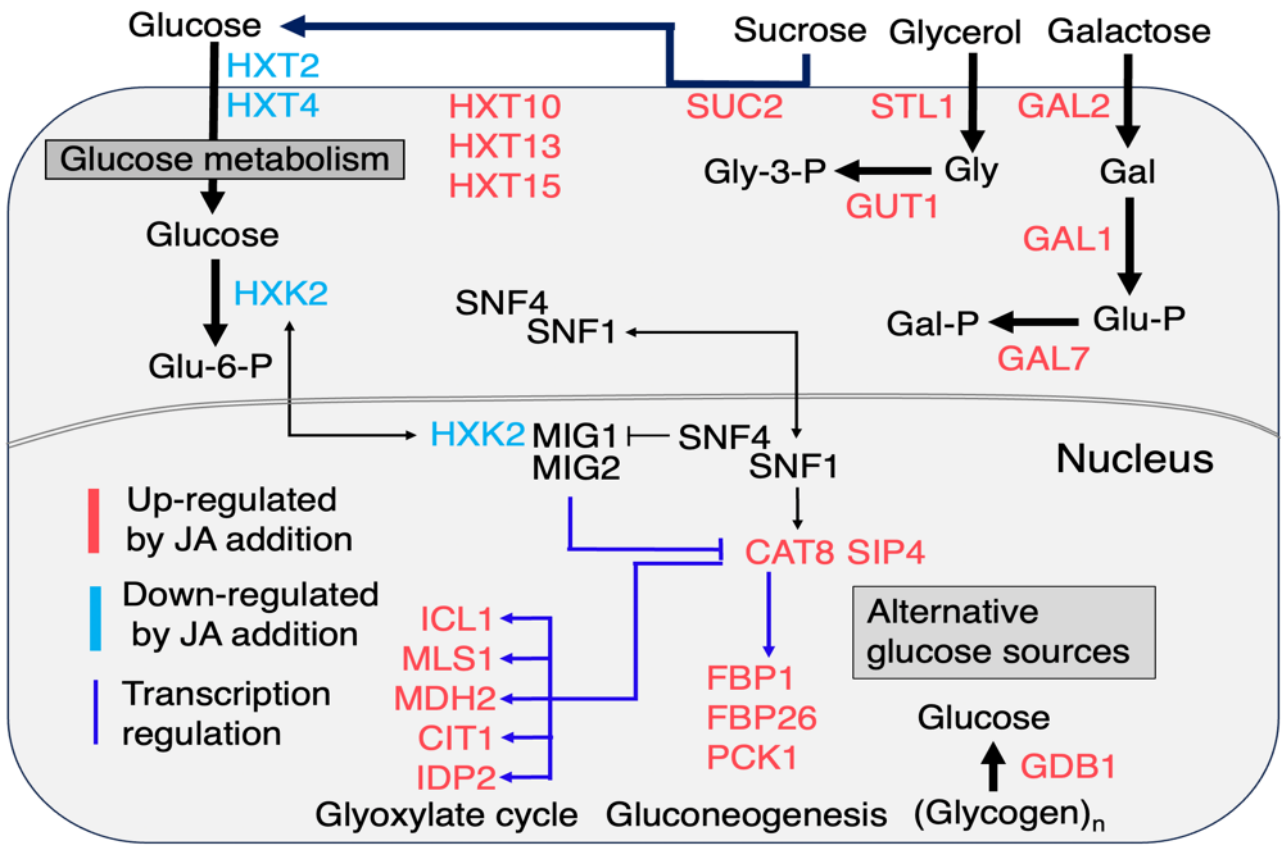

Figure S6. Effect of methyl jasmonate on yeast transcription. A. NCBI common tree of fungi found to respond to methyl-jasmonate. Ascomycota, Basidiomycota, & Mucoromycota phyla are colored respectively. **B.** Left, MeJA-induced gene expression. Left, Volcano plot representation of differentially expressed genes in MeJA-treated relative to DMSO-treated. Dotted lines represent ≥1 and ≤1-fold changes. Labelled red dots depict carbon metabolism-related genes (**see Table S1**). Middle, Over-representation of GO annotated carbon metabolic processes in the presence of MeJA (**see Table S1**). Right comparison of MeJA regulated gene expression to genes regulated by glycerol. **C**. Placement of MeJA regulated genes into sugar metabolism. Left, thick blue arrows: genes transcriptional regulated by MeJA. Red labels; genes activates by MeJA. Blue labels; genes repressed by MeJA addition.

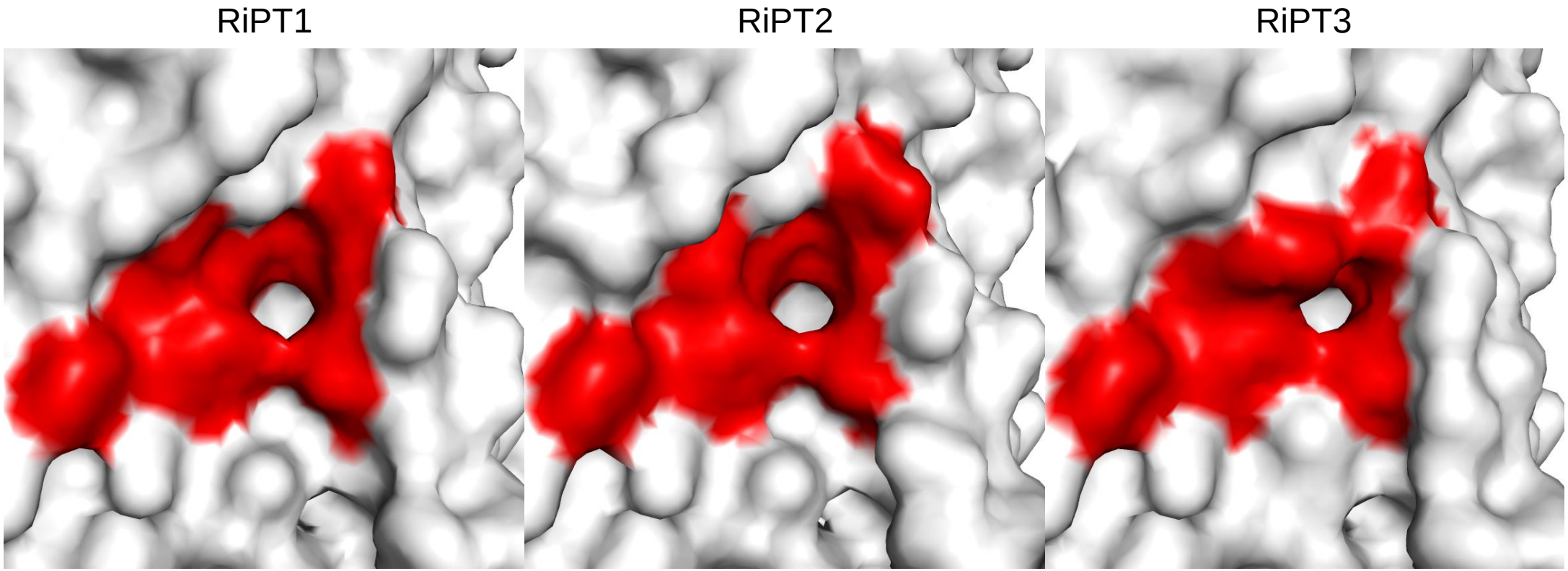

Figure S7. Architecture of binding pockets in three Pho84 homologs from *Rhizophagus irregularis (*RiPT1, RiPT2, RiPT3) modeled on SiPT. RiPT1 and RiPT2 are structurally similar and can accommodate (+)-(*2'R*)-GR24 based on docking simulations. RiPT3 contains an occlusion in the pocket on the left side caused by a Phe at position 212 (amino acid coordinate in ScPHO84), which precludes binding to (+)-(*2'R*)-GR24.

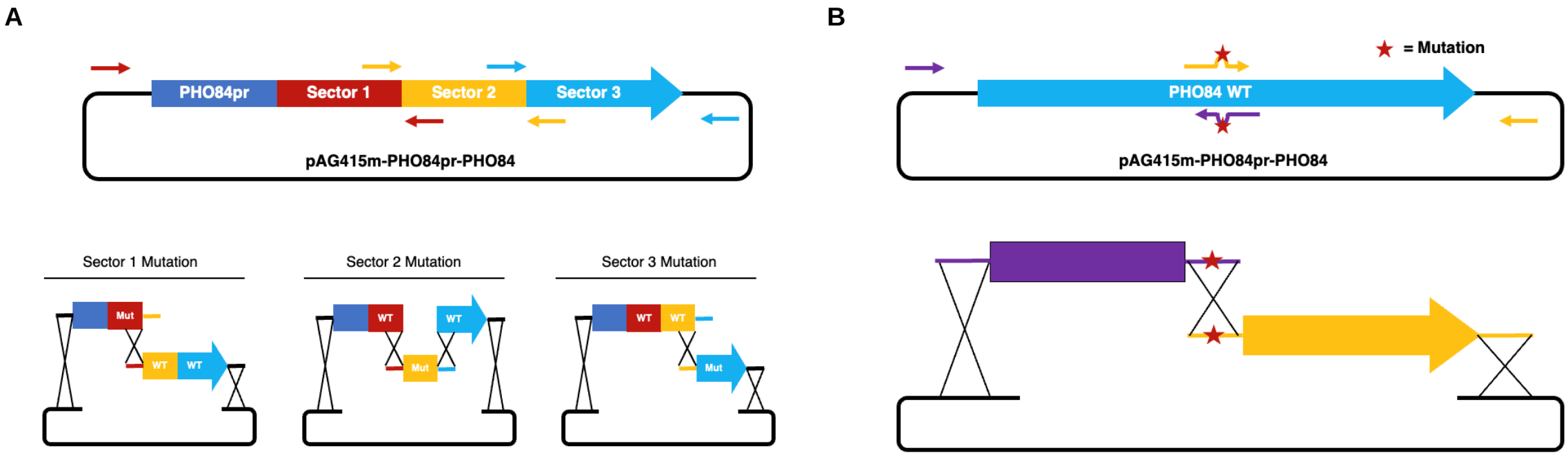

Figure S8. Strategy for determining causative SNPs and PCR-directed mutagenesis A. Strategy for determining the causative SNP underlying strigolactone insensitivity. In some cases, a single mutant *PHO84* allele had multiple SNPs. Thus, to determine which SNP was causative in SL insensitivity, the *PHO84* coding region was first split into three approximately equal sectors and primers were designed to amplify each sector from either the mutant or wildtype *PHO84* (**bottom**). Gap-repair cloning (Joska *et al.* 2014) was then used to re-assemble the full *PHO84* coding region on a plasmid such that it only contained one SNP per construct, which was then re-tested for SL insensitivity. **B.** Strategy for PCR-directed mutagenesis of *PHO84*. Primers were designed to incorporate single amino acid changes into the coding region of *PHO84* (**top**)**.** Gap-repair cloning (Joska *et al*., 2014) was then used to re-assemble the full *PHO84* coding sequence on a plasmid (**bottom**).